Cell

Two Cyclin-Dependent Kinase Pathways Are Essential for Polarized Trafficking of Presynaptic Components

Chan-Yen Ou,[1,5] Vivian Y. Poon,[2,5] Celine I. Maeder,[1] Shigeki Watanabe,[3] Emily K. Lehrman,[1] Amy K.Y. Fu,[4] Mikyoung Park,[1] Wing-Yu Fu,[4] Erik M. Jorgensen,[3] Nancy Y. Ip,[4] and Kang Shen[1,*]
[1]Department of Biology, Howard Hughes Medical Institute, Stanford University, 385 Serra Mall, California 94305, USA
[2]Neurosciences Program, Stanford University School of Medicine, 385 Serra Mall, Stanford, California 94305, USA
[3]Department of Biology, Howard Hughes Medical Institute, University of Utah, Salt Lake City, UT 84112-0840, USA
[4]Department of Biochemistry, Biotechnology Research Institute and Molecular Neuroscience Center, Hong Kong University of Science & Technology, Clear Water Bay, Kowloon, Hong Kong, China
[5]These authors contributed equally to this work
*Correspondence: kangshen@stanford.edu
DOI 10.1016/j.cell.2010.04.011

SUMMARY

Polarized trafficking of synaptic proteins to axons and dendrites is crucial to neuronal function. Through forward genetic analysis in *C. elegans*, we identified a cyclin (CYY-1) and a cyclin-dependent Pctaire kinase (PCT-1) necessary for targeting presynaptic components to the axon. Another cyclin-dependent kinase, CDK-5, and its activator p35, act in parallel to and partially redundantly with the CYY-1/PCT-1 pathway. Synaptic vesicles and active zone proteins mostly mislocalize to dendrites in animals defective for both PCT-1 and CDK-5 pathways. Unlike the kinesin-3 motor, *unc-104/Kif1a* mutant, *cyy-1 cdk-5* double mutants have no reduction in anterogradely moving synaptic vesicle precursors (SVPs) as observed by dynamic imaging. Instead, the number of retrogradely moving SVPs is dramatically increased. Furthermore, this mislocalization defect is suppressed by disrupting the retrograde motor, the cytoplasmic dynein complex. Thus, PCT-1 and CDK-5 pathways direct polarized trafficking of presynaptic components by inhibiting dynein-mediated retrograde transport and setting the balance between anterograde and retrograde motors.

INTRODUCTION

Neurons are highly specialized cells capable of transmitting and processing information through their polarized cellular processes: dendrites receive signals through neurotransmitter receptors and transform these signals into electrical impulses, while axons convert these electrical impulses into chemical signals at presynaptic sites through synaptic vesicle cycles. Therefore, the localization of synaptic vesicles and other active zone components at axonal presynaptic sites is absolutely essential for neuronal function.

How are these axonal or dendritic molecules localized appropriately? There are multiple possible routes that diverge at the levels of sorting, trafficking, and retention (Horton and Ehlers, 2003). Proteins are sorted into different carrier vesicles in the cell body. Certain vesicles are specifically transported to one compartment, while others travel into multiple compartments before being selectively retained in one compartment.

The sheer length of most axons and their lack of protein synthesis machinery demands efficient transport systems to traffic synaptic vesicle precursors (SVPs) and active zone components from the cell body to the axons. Intriguingly, studies in dissociated neuronal cultures showed that several axonal proteins such as synaptic vesicle v-SNARE VAMP2/synaptobrevin, cell adhesion molecule L1/neuron-glia cell adhesion molecule NgCAM, and sodium channel Nav1.2, are initially transported to both the axon and dendrites but later localize to the axon through transcytosis (Burack et al., 2000; Garrido et al., 2001; Sampo et al., 2003; Wisco et al., 2003; Yap et al., 2008). These results indicate that there are trafficking mechanisms both to bring axonal cargo to the dendrite and to transport them into axons.

The microtubule cytoskeleton and related molecular motors are largely responsible for the long-range trafficking of axonal components. Microtubules are oriented plus-end distal in the axon, while they have mixed polarity in dendrites (Baas et al., 1988). The vast majority of the members of the kinesin superfamily move unidirectionally toward the plus end of microtubules, while cytoplasmic dyneins transport cargo in the opposite direction (Hirokawa and Takemura, 2005; Vale, 2003). These molecular motors are highly regulated. They recognize various cargo through direct binding or by utilizing different adaptors. Different adaptors are sufficient to guide motors toward axons or dendrites. Overexpression of the KIF-5-interacting domain of glutamate receptor-interacting protein 1 (GRIP) causes KIF-5 to accumulate in dendrites while overexpression of JIP3/Sunday driver leads to KIF-5

accumulation in axons (Setou et al., 2000). Other regulators can associate with motors and modulate their activity. For example, the retrograde motor dynein and its regulator LIS1 associate with Nudel, a factor phosphorylated by cyclin-dependent kinase-5 (CDK-5) (Niethammer et al., 2000; Sasaki et al., 2000). Inhibiting CDK-5 phosphorylation of NUDEL in vitro disrupts neurite morphology, a defect observed in dynein mutants as well. The tight regulation of motors is not surprising given the wide array of cargo that they transport to diverse locations.

In vivo studies identified two kinesin family motors and the dynein complex to be important for trafficking presynaptic components. UNC-104/Imac/KIF1A, a member of the kinesin-3 family, is the primary motor responsible for transporting SVPs. Mutant worms and flies lacking this gene product show almost complete failure of axonal trafficking—most SVPs accumulate in neuronal cell bodies (Hall and Hedgecock, 1991; Pack-Chung et al., 2007). The conventional kinesin-1/KIF5/KHC also plays a role in this process as it binds SVPs, and disruption of this motor or its adaptor reduces the levels of SVPs and the active zone protein bassoon at presynaptic sites (Cai et al., 2007; Sato-Yoshitake et al., 1992). Third, disrupting components of the cytoplasmic dynein complex leads to misaccumulation of synaptic proteins (Fejtova et al., 2009; Koushika et al., 2004). Taken together, these results indicate that the localization of presynaptic components requires the cooperation of multiple motors. However, how motors are regulated to distinguish between axons and dendrites, how presynaptic cargo is deposited specifically at presynaptic sites, and how different motors interact with one another are important questions that remain to be addressed.

Here, we utilized an in vivo system in *C. elegans* to study the intracellular trafficking of SVPs and active zone proteins. We identified two cyclin-dependent kinase pathways that are essential for axonal localization of presynaptic components. Our results suggest that these kinase pathways regulate the localization of presynaptic components by inhibiting retrograde trafficking that is likely mediated through the dynein motor.

RESULTS

Presynaptic Components Mislocalize to the Dendrite of the DA9 Motor Neuron in *wy575* and *wy302* Mutants

The cholinergic motor neuron DA9 elaborates a morphologically and molecularly distinct axon and dendrite, and is well suited for the study of mechanisms regulating the polarized localization of axonal and dendritic proteins in vivo. We visualized both presynaptic components and dendritic proteins in DA9 using cell-specific promoters (*itr-1 pB* or *mig-13*) to express fluorescently tagged protein markers in vivo. Consistent with electron microscopic reconstruction data (White et al., 1976), synaptic vesicle proteins and active zone markers localize only to a discrete segment of the axon while several proteins localize selectively to the dendrite (Klassen and Shen, 2007; Poon et al., 2008).

To identify factors important for localizing presynaptic components, we visually screened randomly mutagenized animals for mutants with abnormal distribution patterns of presynaptic components. We isolated two mutants with similar and fully penetrant defects with presynaptic markers present in both axons and dendrites. In both *wy575* and *wy302* mutants, synaptic vesicle-associated RAB-3, active zone component SYD-2/liprin-α, synaptic vesicle transmembrane proteins SNB-1/synaptobrevin and SNG-1/synaptogyrin mislocalize to the DA9 dendrite (Figure 1B, Figure 1C, Figure 1H, and Figure 1I compared with Figure 1A and Figure 1G, and Figures S1A–S1L available online). DA9 axonal and dendritic morphology is otherwise normal. Furthermore, the majority of the presynaptic proteins is still distributed in the axon, and these proteins colocalize with one another in the normal synaptic domain (Figures 1H and 1I). These results indicate that except for mislocalized presynaptic components, many aspects of DA9 development, including axon guidance, dendrite outgrowth, and synaptic target selection, are normal in these two mutants. Consistent with this notion, while both *wy575* and *wy302* mutants have slightly lower brood sizes, they are fertile, active, and exhibit largely normal locomotion.

wy575 and *wy302* Are Mutant Alleles of a Cyclin-Dependent Kinase and a Cyclin, Respectively

Using single nucleotide polymorphism mapping, transgenic rescue, and sequence analysis, we mapped the *wy575* mutation to *pct-1*, which encodes a highly conserved Pctaire kinase of the cyclin-dependent kinase family (Figures S1U and S1V). Pctaire kinases have been implicated in neurite outgrowth, exocytosis, and tau phosphorylation (Graeser et al., 2002; Herskovits and Davies, 2006; Liu et al., 2006). cDNA sequences predict three isoforms of PCT-1 with common C-terminal kinase domains and variable N-terminal sequences. *wy575* is a missense mutation of a highly conserved aspartic acid residue in the ATP-binding pocket of the kinase (D377N). We also examined the phenotypes of two different deletion alleles of *pct-1* in DA9: one affects two of the three isoforms (*ok1707)* while the other removes the kinase domain in all three isoforms and is a predicted null (*tm2175)*. *ok1707* mutants have no mislocalization defect, while *tm2175* mutants are indistinguishable from *wy575* mutants (Figure 2J), suggesting that the third isoform is sufficient and that both *wy575* and *tm2175* are likely null alleles.

Using similar methods, we mapped *wy302* at the genetic locus ZK353.1. This gene encodes two highly similar isoforms containing a predicted cyclin domain. It is orthologous to mammalian cyclin Y that has not been studied previously (Figures S1X and S1Y). We named the gene CYY-1 (Cyclin Y). The *wy302* allele results in a stop codon in the ninth amino acid and likely represents a null allele.

PCT-1, CYY-1, CDK-5, and CDKA-1/p35 Act Cell Autonomously in DA9 to Ensure the Polarized Localization of Presynaptic Components

Since the phylogenetic analysis shows that PCT-1 is most closely related to CDK-5 (Figure S1U), we further exam CDK-5 and other CDK mutants. While mutations in CDK-1, CDK-7, and CDK-8 have no effect (data not shown), null mutations in *cdk-5* or its activator *cdka-1/p35* lead to dendritic accumulation of presynaptic components (Figures 2A and 2B, Figure S1). Like the *pct-1* and *cyy-1* mutants, this

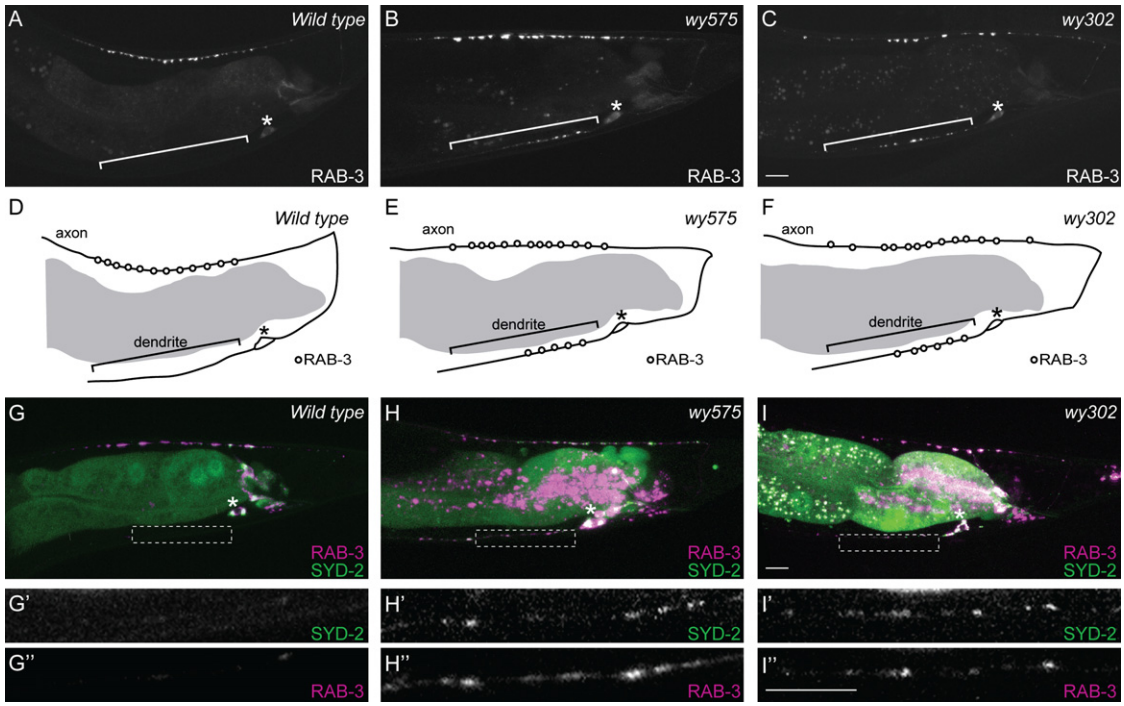

Figure 1. Synaptic Vesicle-Associated RAB-3 and Active Zone Protein SYD-2/Liprin-α Mislocalize to the DA9 Dendrite in *wy575* or *wy302* Mutants

(A) A wild-type adult expressing GFP::RAB-3 in DA9(*wyIs85*).

(B and C) Two mutants expressing GFP::RAB-3.

(D–F) Schematic diagrams of GFP::RAB-3 distribution.

(G–I) Wild-type (G) and mutant animals (H and I) coexpressing GFP::SYD-2/liprin-α and mcherry::RAB-3(*wyEx2055*). (G'-I', G''-I'') Higher magnification micrographs of the corresponding dotted boxes. The fluorescence in the middle of the worm is gut autofluorescence. Anterior, left; and dorsal, top. Bracket, dendrite; asterisk, above cell body.

The scale bar represents 10 μm. See also Figure S1.

mislocalization defect in *cdk-5* or *cdka-1/p35* mutants is fully penetrant. The mutant animals have normal DA9 guidance and morphology, and do not exhibit obvious defects in locomotory behavior.

We subsequently determined if these four genes are expressed endogenously in DA9. Cytoplasmic fluorophore under the control of their endogenous promoters, revealed fluorescence in DA9 as well as other ventral cord motor neurons (data not shown). CYY-1 is also expressed in other tissues such as the gut and gonad. Using the *itr-1 pB* promoter that drives expression specifically in DA9 in the tail, we asked if DA9-specific expression of each gene is sufficient to rescue the mislocalization defect of SVPs. For each gene, we generated two independent transgenic strains expressing the corresponding cDNA or genomic fragment in DA9. Expression of these four genes in DA9 almost completely rescues the mutant phenotype, suggesting that PCT-1, CYY-1, CDK-5, and CDKA-1/p35 act cell-autonomously in DA9 (Figure 2C).

PCT-1, CYY-1, CDK-5, and CDKA-1/p35 Act in Parallel Pathways

Since *pct-1, cyy-1, cdk-5,* and *cdka-1/p35* mutants have similar defects, we investigated their genetic relationships. Using putative null mutants, we generated all six combinations of double mutants and compared them with the single mutants (Figures 2D–2I). Quantitative analysis of GFP::RAB-3 distribution in the DA9 axon and dendrite showed that between 19%–47% of total RAB-3 fluorescence is present in the dendrite of these single mutants compared to 0.3% in wild-type animals (Figure 2J). As *cyy-1; pct-1* double mutant animals are indistinguishable from each single mutants, PCT-1 and CYY-1 likely function in the same genetic pathway. Likewise, *cdka-1/p35 cdk-5* double mutant animals have a mislocalization defect similar to *cdk-5* single mutants, a result one would expect if CDKA-1/p35 activates CDK-5.

The other four double mutants, on the other hand, exhibit dramatically enhanced mislocalization defects. Nearly all SVPs (86%–98%) are present in the DA9 dendrite in the *cdk-5; pct-1, cdka-1/p35; pct-1, cyy-1 cdk-5,* and *cdka-1/p35 cyy-1* double mutants (Figures 2F–2J). The active zone protein SYD-2/liprin-α is similarly dramatically mislocalized in these double mutants, suggesting that trafficking and localization of multiple presynaptic components are defective (Figure S2). To address if these defects are specific to the cholinergic DA9 neuron, we examined the localization of synaptic vesicle-associated RAB-3 in other neurons. We found that the GABAergic DD motor neurons and

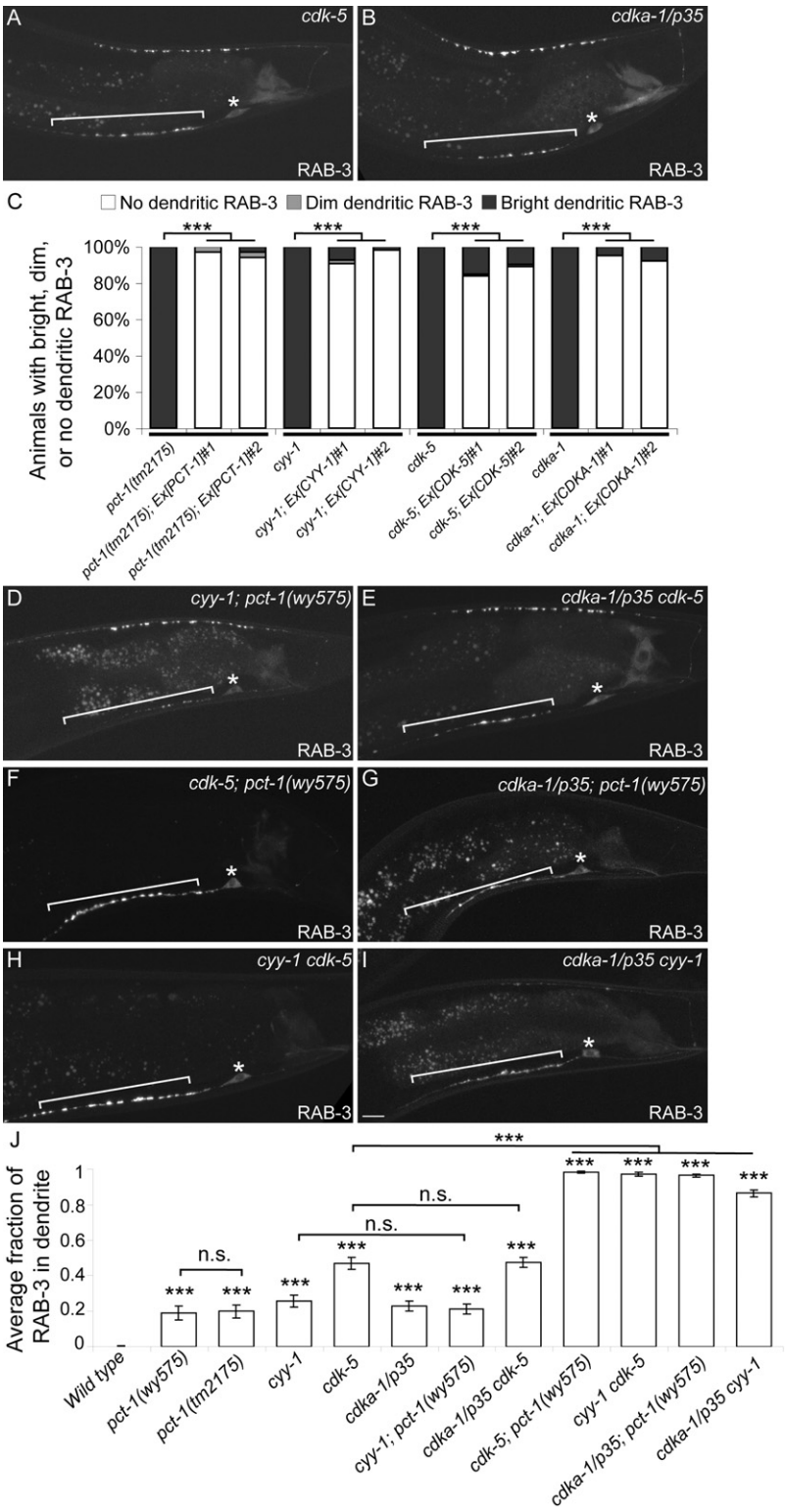

Figure 2. PCT-1, CYY-1, CDK-5, and CDKA-1/p35 Act in Two Pathways in DA9

(A and B) *cdk-5(ok626)* (A) or *cdka-1/p35(tm648)* (B) mutant animal expressing GFP::RAB-3(*wyIs85*). Bracket, dendrite; asterisk, above cell body.

(C) DA9-specific expression of the four genes rescues the GFP::RAB-3(*wyIs85*) mislocalization defect (*wyEx2286-9,2860-1*). n = 100. ***$p < 0.0001$. χ^2 test.

(D–I) Double mutants expressing GFP::RAB-3. Bracket, dendrite; asterisk, above cell body. The scale bar represents 10 μm.

(J) Graph of severity of GFP::RAB-3 mislocalization. Error bars represent the standard error of the mean (SEM). n = 20. ***$p < 0.0001$ compared with *wild-type*. n.s., not significant. t test.

See also Figure S2.

the RIA interneurons are also severely affected in *cyy-1 cdk-5* double mutants and GFP::RAB-3 mislocalizes to dendrites or dendritic segments (Figure S3). Intriguingly, the localization of synaptic vesicle markers in the cholinergic DB motor neurons is only mildly affected in *cyy-1 cdk-5* double mutants (data not shown), suggesting that these two pathways are required for many but not all neurons. Not surprisingly, these four double mutants are largely paralyzed, indicating a loss of functional synapses in motor neurons. These results are consistent with *pct-1* and *cyy-1* acting in a pathway parallel to *cdk-5* and *cdka-1/p35* in multiple neurons. The observed drastic enhancement further highlights that these two pathways are essential for the polarized localization of presynaptic components.

To definitively understand the synaptic structural defects in the *cyy-1 cdk-5* double mutants, we reconstructed segments (4–7μm) of the dorsal nerve cord using serial electron microscopy (EM) from three *cyy-1 cdk-5* double mutant animals and three wild-type control animals. Consistent with our findings with fluorophore-tagged synaptic markers, we found that the number of synaptic vesicles and active zones in the DA and DD axons are significantly reduced whereas presynaptic specializations in the DB neurons appear normal (Figure 3 and unpublished data, S.W. and K.S.). Since the reconstruction was performed where the DA1 to DA4 neurons form synapses, the synaptic vesicle localization defect in DA neurons is not limited to DA9, but is true for the anterior DA neurons as well. This EM analysis also revealed that the size and appearance of the synaptic vesicles in *cyy cdk-5* mutants is indistinguishable from that in wild-type controls. Furthermore, the appearance of the muscle arms and their contacts with the motor neurons are largely normal, arguing that the wiring of the motor circuits remains intact in the mutant animals (data not shown).

The close phylogenetic relationship, the similarity of their loss-of-function phenotypes, and the enhanced phenotype of the

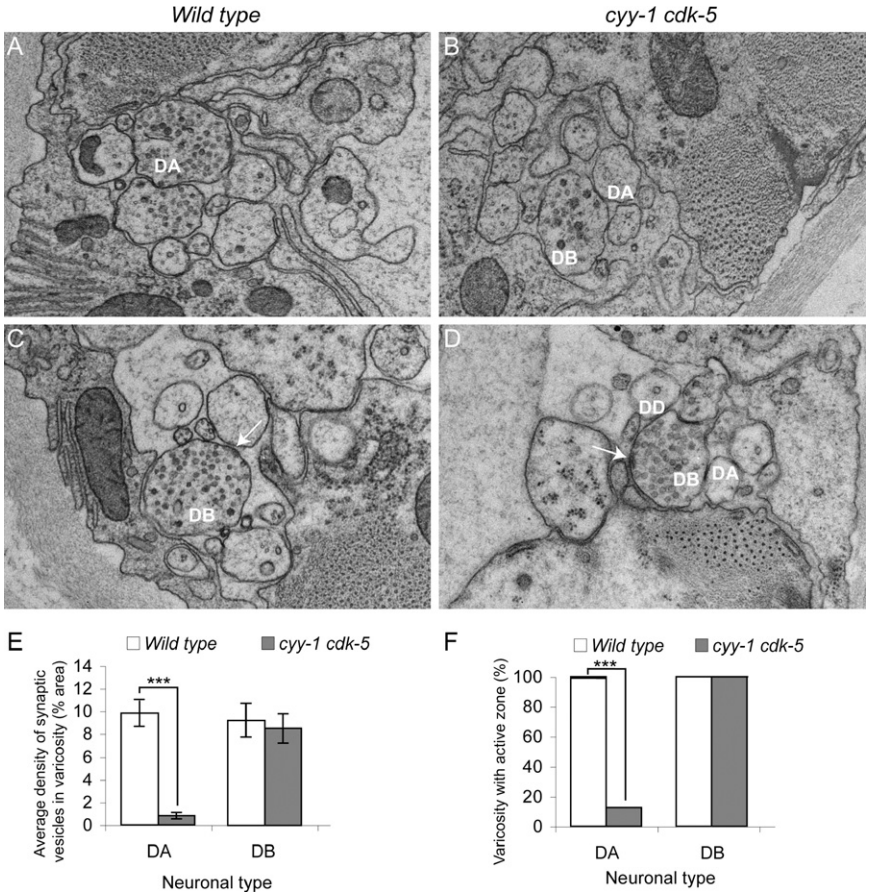

Figure 3. The Number of Synaptic Vesicles and Active Zones is Reduced in the Dorsal Axons of DA Neurons in *cyy-1 cdk-5* Double Mutants

(A–F) Representative EM images of varicosities of DA (A and B) and DB (C and D) neurons in wild-type (A and C) or *cyy-1 cdk-5* mutant animals (B and D). Arrows, active zones. (E) Graph of average density of synaptic vesicles in each varicosity in DA and DB neurons. Error bars represent SEM. Number of varicosities = 4 - 8. ***$p < 0.0005$. t test. (F) Graph of varicosities with active zones in DA and DB neurons. Number of varicosities = 4 – 8. ***$p < 0.0001$. χ^2 test. See also Figure S3.

double mutants indicate that the PCT-1 and CDK-5 pathways might perform similar and redundant functions in DA9. To directly address this, we examined if over-activating one pathway could compensate for the loss of the other pathway. Indeed, we found that overexpression of PCT-1 in *cdk-5* mutants significantly rescues their mislocalization defects, and likewise, overexpression of CDK-5 significantly rescues defects of *pct-1* mutant animals (Figure 4A).

CYY-1 Acts as an Essential Activator of PCT-1

While it is well established that p35 directly binds to and activates CDK-5 (Lew et al., 1994; Tsai et al., 1994; Uchida et al., 1994), the interaction between CYY-1 and PCT-1 has not been studied. No vertebrate cyclin is known to activate Pctaire kinases (Liu et al., 2006). We therefore tested if CYY-1 associates with and activates PCT-1 using tagged recombinant CYY-1 and PCT-1 in 293T cells. We observed that CYY-1 and PCT-1 robustly coimmunoprecipitate with each other regardless of the tag we used to perform the pull-down experiment (Figure 4B). Furthermore, the kinase activity of PCT-1 is strictly dependent on the presence of CYY-1 (Figure 4C). Consistently, overexpression of functional PCT-1 completely fails to rescue the *cyy-1* mutants, indicating that the function of PCT-1 depends on CYY-1 (Figure 4D). These results strongly suggest that CYY-1 directly binds and activates PCT-1 to regulate the localization of presynaptic components.

If PCT-1 is the only downstream factor of CYY-1, CYY-1 should have no activity in *pct-1* null mutant animals. However, we observed that overexpression of CYY-1 significantly rescues the mislocalization defect in *pct-1(tm2175)* mutant animals (Figure 4D). This indicates that overexpression of CYY-1 can affect the localization of presynaptic components through a mechanism independent of PCT-1. A primary candidate is CDK-5 since it is closely related to PCT-1 and we observed that the CDK-5 transgene that robustly rescues *pct-1* mutant animals only marginally rescues *cyy-1* mutant animals (Figure 4A). As presented in Figure 4D, the CYY-1 transgene that rescues the mislocalization defect in *pct-1* mutants completely fails to rescue the mislocalization defect in *cdk-5; pct-1* or *cdka-1/p35; pct-1* double mutants. Taken together, these genetic interaction studies indicate that CYY-1 acts upstream of PCT-1 and can also potentially activate the CDKA-1/p35-CDK-5 pathway.

To further test whether CYY-1 can directly activate CDK-5, we performed in vitro kinase assays. We found that the kinase activity of CDK-5 can indeed be stimulated by CYY-1 suggesting that CYY-1 might also be an activator of CDK-5 (Figure S4A).

Subcellular Localization of PCT-1, CYY-1, CDK-5, and CDKA-1/p35

Next, we examined the subcellular localization of PCT-1, CYY-1, CDK-5, and CDKA-1/p35. We found that CDK-5::YFP predominantly localizes to presynaptic sites and is present as faint puncta in the dendrite (Figure S4C). CDKA-1/p35::YFP shows a presynaptic distribution in the axon and a punctate localization pattern in the dendrite (Figure S4E). The localization of CDK-5 is completely dependent on UNC-104/KIF1A (data not shown). Consistent with the presynaptic localization of the vertebrate CDK-5 (Tomizawa et al., 2002), these two distribution patterns suggest that CDK-5 and CDKA-1/p35 are likely to be associated with presynaptic components.

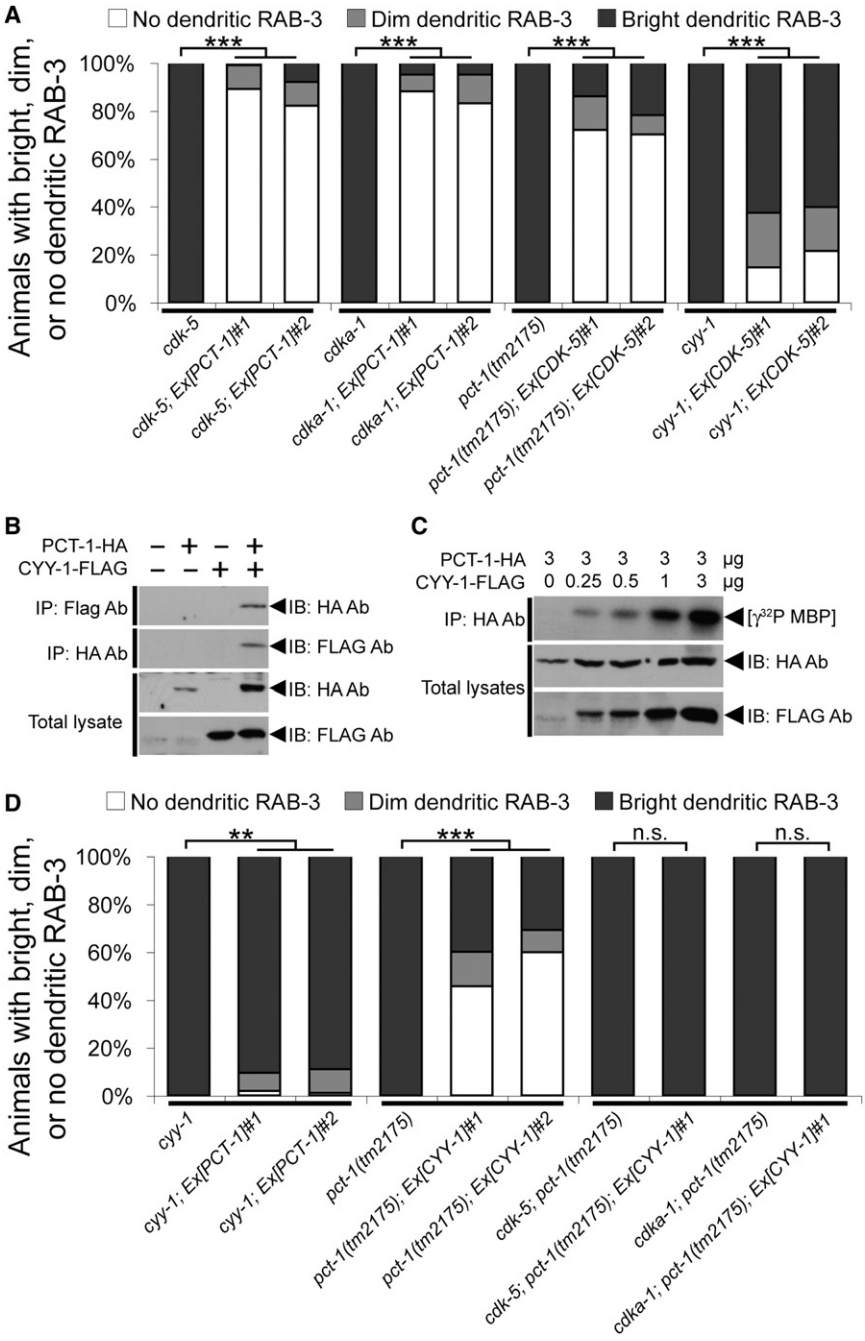

Figure 4. CYY-1 Activates PCT-1 and Possibly CDK-5

(A) PCT-1 or CDK-5 suppresses the GFP::RAB-3 mislocalization defects in *cdk-5* and *cdka-1/p35* mutants or *pct-1* and *cyy-1* mutants respectively (*wyEx2506-7,2624,2626*). n = 100. ***p < 0.0001. χ^2 test.

(B and C) PCT-1-HA and/or CYY-1-FLAG were coexpressed in 293T cells as indicated. (B) Lysates were coimmunoprecipitated with HA and FLAG antibodies, and then immunoblotted with FLAG and HA antibodies respectively. (C) PCT-1 was coimmunoprecipitated with HA antibody and kinase activity was measured in vitro using myelin basic protein (MBP) as substrate.

(D) *pct-1* weakly suppresses the *cyy-1* defect, while *cyy-1* partially suppresses the *pct-1* defect in a CDK-5 or CDKA-1/p35-dependent manner (*wyEx2506-7,2776-7*). n = 100. ***p < 0.0001. **p < 0.001. n.s., not significant. χ^2 test.

See also Figure S4.

Interestingly, CDK-5 and PCT-1 have very different localization patterns. PCT-1::GFP is diffusely localized within DA9 and labels both the dendrite and axon evenly (Figure S4B). CYY-1::YFP is also present in both axons and dendrites, but is enriched in the dendrite and proximal axon (Figure S4D). Taken together, if CYY-1 is required for the activity of PCT-1, one would imagine that the activity of PCT-1 is highest in the dendrite and lowest in the synaptic domain and distal axon.

Collectively, these data suggest that although both PCT-1 and CDK-5 affect similar biological processes, their exact cell biological functions in vivo might be different. However, they can substitute for each other when overexpressed in the single mutant background.

Dendritic Mislocalization of Presynaptic Components in CDK Mutants Is Unlikely to Be Caused by Axon-Dendrite Specification or Synapse Assembly Defects

After establishing the genetic and biochemical interactions between PCT-1, CYY-1, CDK-5, and CDKA-1/p35, we considered the following three possibilities that may lead to dendritic presynaptic components: (1), a defect in axon-dendrite specification; (2), a failure of local assembly at presynaptic specializations; and (3), an impairment of intracellular transport of presynaptic components.

To address the first possibility, we examined DA9 axonal and dendritic guidance and outgrowth, trafficking of plus- and minus-end directed motors, dendritic proteins, and a non-synaptic axonal cargo. Both the timing and directionality of axonal and dendritic outgrowth are normal in *cyy-1 cdk-5* double mutants (Figures S5A–S5D, data not shown). The overall MT organization in both the axon and dendrite is generally unaltered in the absence of the CDK pathways assayed by the subcellular distribution of MT-based motors (Figures S5E–S5H). Futhermore, we examined four dendritic proteins including CAM-1/ROR receptor tyrosine kinase, UNC-9/innexin, DYS-1/dystrophin, and fibrillin (Poon et al., 2008; Sieburth et al., 2005) and they localize nomally to dendrites in *cyy-1 cdk-5* mutant

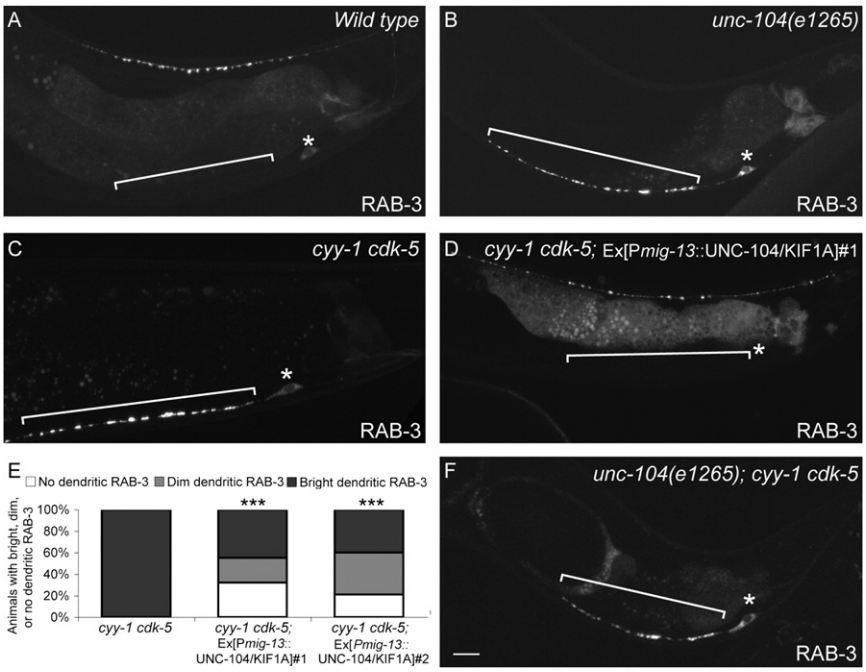

Figure 5. The CDKs Affect Axonal Transport of Presynaptic Components

(A and B) Wild-type (A) or *unc-104/kif1a* mutant animal (B) expressing GFP::RAB-3(*wyIs85*). RAB-3 is only present in the cell body and dendrite in the *unc-104/kif1a* mutant animal.

(C and D) *cyy-1 cdk-5* mutant animal expressing GFP::RAB-3 in the absence (C) or presence (D) of an *unc-104/kif1a* transgene expressed in DA9(*wyEx2694*).

(E) UNC-104/KIF1A partially suppresses the GFP::RAB-3 mislocalization defect in *cyy-1 cdk-5* mutant animals. n > 100. ***p < 0.0001. χ^2 test.

(F) GFP::RAB-3 in *unc-104/kif1a; cyy-1 cdk-5* mutant animal. Bracket, dendrite; asterisk, above cell body.

The scale bar represents 10 μm. See also Figure S5.

animals (Figures S5I–S5P). Glutamate receptor localizes to dendrite of another neuron RIA, further indicating that trafficking of dendritic cargo is unaffected (Figure S3H and Figure S3K). Lastly, we investigated if other axonal cargo are trafficked normally. TOM20, a subunit of the mitochondrial translocase complex, remains present in the axon in *cyy-1 cdk-5* mutant animals (Figures S5Q and S5R), suggesting that non-presynaptic axonal cargo continues to be trafficked appropriately to the axon. Taken together, our data suggest that general axon and dendrite specification is normal in the absence of the CDK pathways and that the CDKs specifically affect localization of presynaptic components and not other axonal or dendritic cargo.

Is the failure of local assembly at presynaptic specializations the direct cause for dendritic mislocalization of presynaptic components in *cdk-5* or *pct-1* mutant? Since *cdk-5* or *pct-1* single mutants have a relatively normal accumulation of RAB-3 in the presynaptic region compared with the *syd-1; syd-2/liprin-α* double mutants that have severe presynaptic assembly defects in DA9 whereas *cdk-5* or *pct-1* single mutants exhibit much more severe accumulation of RAB-3 in the dendrites, there is no correlation between defective presynaptic assembly and the accumulation of stable RAB-3 puncta in the dendrite (Figures S5S and S5T). It is thus unlikely that the assembly defect alone can fully account for the dramatic mislocalization of presynaptic components in *cyy-1 cdk-5* double mutants.

We then considered the third possibility that the CDK pathways regulate intracellular transport of presynaptic components. Since intracellular transport occurs continuously throughout the life of the neuron, we expect the CDKs to be required continuously if they regulate transport. Using a temperature-dependent silencing strategy (Poon et al., 2008), we observed that disruption of PCT-1 or CDK-5 late in development is sufficient to mislocalize SVPs to the dendrite. In addition, rescuing PCT-1 or CDK-5 late in development is sufficient to partially remove ectopic SVPs from the dendrite (Figures S6A–S6C). These findings suggest that both CDKs are required to maintain the polarized localization of SVPs and that this defect is reversible.

PCT-1 and CDK-5 Genetically Interact with the Kinesin Motor UNC-104/KIF1A

To further understand how the CDK pathways regulate molecular transport, we examined the primary motor responsible for SVP transport, UNC-104/KIF1A, in greater depth. Consistent with previous reports (Hall and Hedgecock, 1991), we found that RAB-3 is completely absent from the axon of *unc-104* mutants, suggesting that UNC-104 is the key anterograde motor responsible for the axonal transport of SVPs. Surprisingly, we also found that SVPs dramatically accumulate in the DA9 cell body and dendrite of *unc-104* mutants, a phenotype similar to that observed in *cyy-1 cdk-5* double mutants (Figure 5B). This distribution pattern indicates that there might be another motor that transports SVPs into the dendrite in the absence of the UNC-104 motor. The similar phenotypes caused by disrupting both CDK pathways or by mutations in UNC-104 suggest that they might be involved in the same biological process. Consistent with this notion, the *unc-104; cyy-1 cdk-5* triple mutants are indistinguishable from the *unc-104* single mutant (Figure 5F).

To further understand the relationship between UNC-104 and the CDK pathways, we overexpressed UNC-104 in the absence of both CDK pathways. As seen in Figures 5D and 5E, UNC-104 expression leads to a partial suppression of the dendritic RAB-3 phenotype. In about 30% of the animals, the dendritic RAB-3 signal is completely absent, suggesting that overproduction of UNC-104 can partially compensate for the loss of both CDK pathways by trafficking SVPs to the axon (Figure 5E). However, despite the absence of dendritic RAB-3 in these animals, their dorsal axonal RAB-3 distribution is still significantly different from that in wild-type animals (Figure 5D). There are fewer and

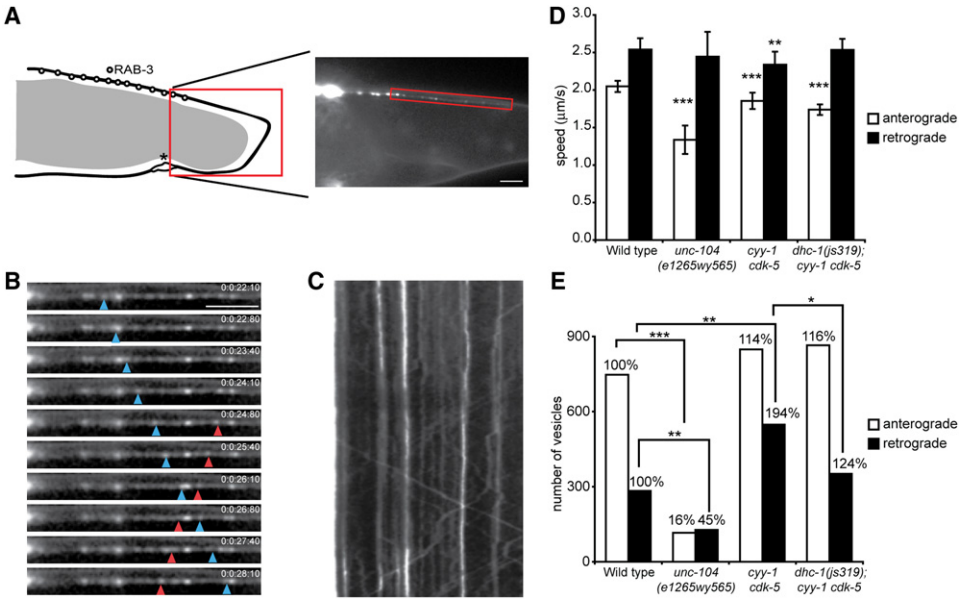

Figure 6. The CDKs Inhibit Retrograde Transport of Presynaptic Components

(A) Left: Schematic diagram of the DA9 neuron and the localization of RAB-3. Right: Representative image of GFP::RAB-3(*wyEx2793*) signal in the dorsal asynaptic domain, where movies were taken.

(B) Image sequence visualizing moving GFP::RAB-3 puncta (blue arrowhead points to a retrogradely moving puncta while red arrowhead corresponds to anterogradely moving puncta). The scale bar represents 5 μm.

(C) Kymograph of the movie shown in (B).

(D) Quantification of vesicle speeds in anterograde and retrograde direction in wild-type, *unc-104(e1265wy565)*, *cyy-1 cdk-5,* and *dhc-1(js319); cyy-1 cdk-5* mutant animals. All three mutants show a decrease in anterograde velocity. Error bars represent SEM. ***p < 0.0001. t test.

(E) Absolute numbers of vesicles moving in an anterograde or retrograde direction. Numbers above the bars represent percentages in relation to *wild-type*. While *unc-104(e1265wy565)* mutants show a dramatic decrease in the number of anterogradely- and retrogradely-moving vesicles, *cyy-1 cdk-5* mutant animals show a significant increase in retrograde transport. ***p < 0.0005; **p < 0.005; *p < 0.05, Wilcoxon rank sum test.

See also Figure S6.

dimmer RAB-3 puncta, which are spread over a larger than normal segment of the dorsal axon. Though these results suggest that the CDKs are likely also involved in events distinct from UNC-104-mediated anterograde transport, they are consistent with the CDK pathways affecting intracellular transport of presynaptic components.

PCT-1 and CDK-5 Inhibit Retrograde Transport of SVPs

To further elucidate how the CDK pathways affect intracellular transport, we performed time-lapse imaging experiments to visualize transporting SVPs in DA9 in vivo. We found that there are numerous small RAB-3 puncta in the axonal segment between the cell body and the dorsal synaptic domain (Figure 6A). These dim puncta are often motile during imaging sessions that last up to a minute, unlike synaptic RAB-3 puncta that remain stable over several days (data not shown). These motile RAB-3 puncta are missing from the axon in *unc-104* mutants, suggesting that trafficking utilizes the same molecular motor as the synaptic vesicles. Hence, we hypothesize that these small puncta represent motile SVPs during axonal transport.

Time-lapse imaging experiments were performed on the dorsal asynaptic segment of the axon immediately proximal to the synaptic region of DA9 (Figures 6A–6C). Measurements in wild-type animals revealed that 76% of the movements are toward the distal axon (anterograde), while 24% of the moving events are retrograde. The average speed of anterograde events is 1.9 μm/s, similar to the speed of dense core vesicles measured in vivo in *C. elegans* (Zahn et al., 2004). The average speed of the retrograde movements is 2.3 μm/s, similar to the speed of the retrograde motor dynein in living *Dictyostelium* cells (Ma and Chisholm, 2002). In order to understand if UNC-104 mediates anterograde movements, we measured the speed of anterograde events in a hypomorphic allele *unc-104(e1265wy565)*. We found that only the speed of anterograde movements, but not retrograde events, is drastically reduced, suggesting that UNC-104 mediates anterograde movements (Figure 6D).

Besides the speed, we also measured the absolute number of anterograde and retrograde movement events. In *unc-104(e1265wy565)* mutants, the absolute number of anterograde events is drastically reduced, consistent with a weakened anterograde motor. Retrograde movement is also reduced, but to a lesser extent, probably due to the reduction of available SVPs to be measured in the mutant axon. Unlike *unc-104(e1265wy565)* mutants, the number of anterograde events is not significantly altered in *cyy-1 cdk-5* double mutants. Instead, we observed a dramatic increase in retrograde events (194% compared with *wild-type*, Figure 6E). Other dynamic

parameters such as the run length and the pause rate remain unaffected in the *cyy-1 cdk-5* double mutant (data not shown). Though *unc-104(e1265wy565)* mutants exhibit a severe impairment in anterograde SVP transport judging from the speed and number of anterograde events (Figures 6D and 6E), there is still significantly more RAB-3 signal in the *unc-104(e1265wy565)* mutant axon compared with the *cyy-1 cdk-5* double mutant (Figure S6D-E). Based on these data, it is more likely that the dramatic increase in retrograde events in *cyy-1 cdk-5* double mutants leads to an imbalance between anterograde and retrograde trafficking, ultimately resulting in failed assembly of presynaptic specializations in the axon and ectopic accumulation of presynaptic components in the dendrite. Similar dynamic measurements in *cdk-5* or *cyy-1* single mutants also reveal imbalanced trafficking with an abnormally high ratio of retrograde events. The amplitude of the defect in single mutants is smaller compared with that of the double mutants (Figure S6F). Hence, we hypothesize that the CDK pathways promote axonal transport by inhibiting retrograde transport. The most direct prediction of this hypothesis is that mutations in a retrograde motor should suppress the mislocalization defect in the CDK mutants.

PCT-1 and CDK-5 Likely Regulate SVP Transport by Inhibiting the Cytoplasmic Dynein Complex

To further identify other downstream components of the CDK pathways, we conducted an unbiased *cdk-5* suppressor screen and isolated five mutants with little or no dendritic RAB-3 in the *cdk-5* mutant background. Four belong to a single complementation group and we mapped one of the four, *wy622*, which turned out to be a mutant allele of *DHC-1*, which encodes *C. elegans* ortholog of the heavy chain of the retrograde motor dynein (Figure 7A). Sequence analysis revealed that *wy622* represents a point mutation in a conserved leucine residue in N-terminal region 2, while the previously characterized but unsequenced loss-of-function allele *js319* represents a splice acceptor mutation at the end of intron 12 in the C-terminal conserved region (Figure 7A) (Koushika et al., 2004). We generated *dhc-1; cdk-5* and *dhc-1; pct-1* double mutants with the *js319* allele. Similar to the *wy622* allele, the *js319* allele completely suppresses the dendritic accumulation of SVPs in either *cdk-5* or *pct-1* single mutants (Figures 7B and 7C). The *dhc-1(js319)* mutant also strongly suppresses the severe dendritic RAB-3 defect and reduces the number of retrogradely moving SVPs in *cyy-1 cdk-5* double mutant animals (Figure 7E, Figure 7J, and Figure 6E). These results suggest the CDK pathways promote axonal transport by inhibiting dynein-mediated retrograde movement in wild-type animals.

NUD-2 Likely Acts Downstream of CDK-5 and PCT-1

To further establish the mechanistic link between the CDK-5 pathways and the cytoplasmic dynein complex, we considered NUD-2 as a direct target. NUD-2 is the worm ortholog of Nudel, a component of the cytoplasmic dynein complex that has been demonstrated as a substrate of CDK5 in vertebrate system (Niethammer et al., 2000; Sasaki et al., 2000). Indeed, we found that the null *nud-2*(*ok949*) allele completely suppresses the dendritic localization of SVPs in *cdk-5* or *pct-1* single mutants, and significantly suppresses the mislocalization phenotype in the *cyy-1 cdk-5* double mutants (Figures 7F–7J). This suppression by *nud-2* is indistinguishable compared with the suppression by *dhc-1*. These results indicate that both DHC-1 and NUD-2 function downstream of the CDK-5/PCT-1 pathways and that CDK-5 and PCT-1 inhibit the activity of the cytoplasmic dynein complex (Figure 7K).

DISCUSSION

Our genetic and imaging experiments provide us with the following model: The axonal MTs are uniformly oriented with their plus-ends toward the axonal tip, while dendrites have mixed polarity with the preferred orientation being minus-ends toward the distal dendrite. Two antagonistic forces determine the localization of presynaptic components: the anterograde motor UNC-104/KIF1A transporting SVPs toward the axonal tip and the retrograde motor dynein trafficking SVPs toward the distal dendrite. PCT-1 and CDK-5 regulate the balance between the anterograde and retrograde trafficking, most likely by inhibiting dynein activity. In wild-type animals, PCT-1 and CDK-5 suppress dynein-mediated transport toward the dendrite, allowing the UNC-104 motor to dominate and achieve the axonal localization of presynaptic components. When both CDK pathways are defective, dynein activity is abnormally high, driving presynaptic components to dendrites.

CYY-1 Activates PCT-1 and Functions in Localizing Presynaptic Components

Although a large body of evidence implicates cyclins in cell cycle regulation, there are some exceptions. For example, D-type cyclins are upregulated in differentiating hematopoietic cells, quiescent myotubes, or in fibroblasts undergoing growth arrest, suggesting their non-mitogenic roles (Furukawa et al., 2000; Kiess et al., 1995; Meyyappan et al., 1998). Our findings suggest a post-mitotic role for CYY-1 in regulating intracellular transport and excluding presynaptic components from the DA9 dendrite. Like the D-type cyclins, CYY-1 may respond to extracellular cues by regulating signal transduction. Identifying the extrinsic signals important for the activity of CYY-1 would provide insight into the pathway that regulates the localization of presynaptic components.

Unlike CYY-1, the mammalian homologs of PCT-1 have been identified and characterized by several groups. Pctaire1, the best-characterized member of this kinase family, regulates neurite outgrowth in the Neuro2A neuroblastoma cell line (Graeser et al., 2002). Pctaire2 is associated with Trap (tudor repeat associator with Pctaire 2) and ik3-1/cables, the adaptor that functionally connects c-abl and CDK-5 to support neurite growth (Yamochi et al., 2001). The third member of this family, Pctaire3, is implicated in cytoskeletal regulation where it indirectly stimulates the phosphorylation of the MT associated protein, tau (Herskovits and Davies, 2006). However, the in vivo functions of these kinases and how they are regulated are poorly understood. Here we show genetically that *cyy-1* falls in the same pathway with *pct-1*. We further show biochemically that CYY-1 binds to and activates PCT-1. It remains

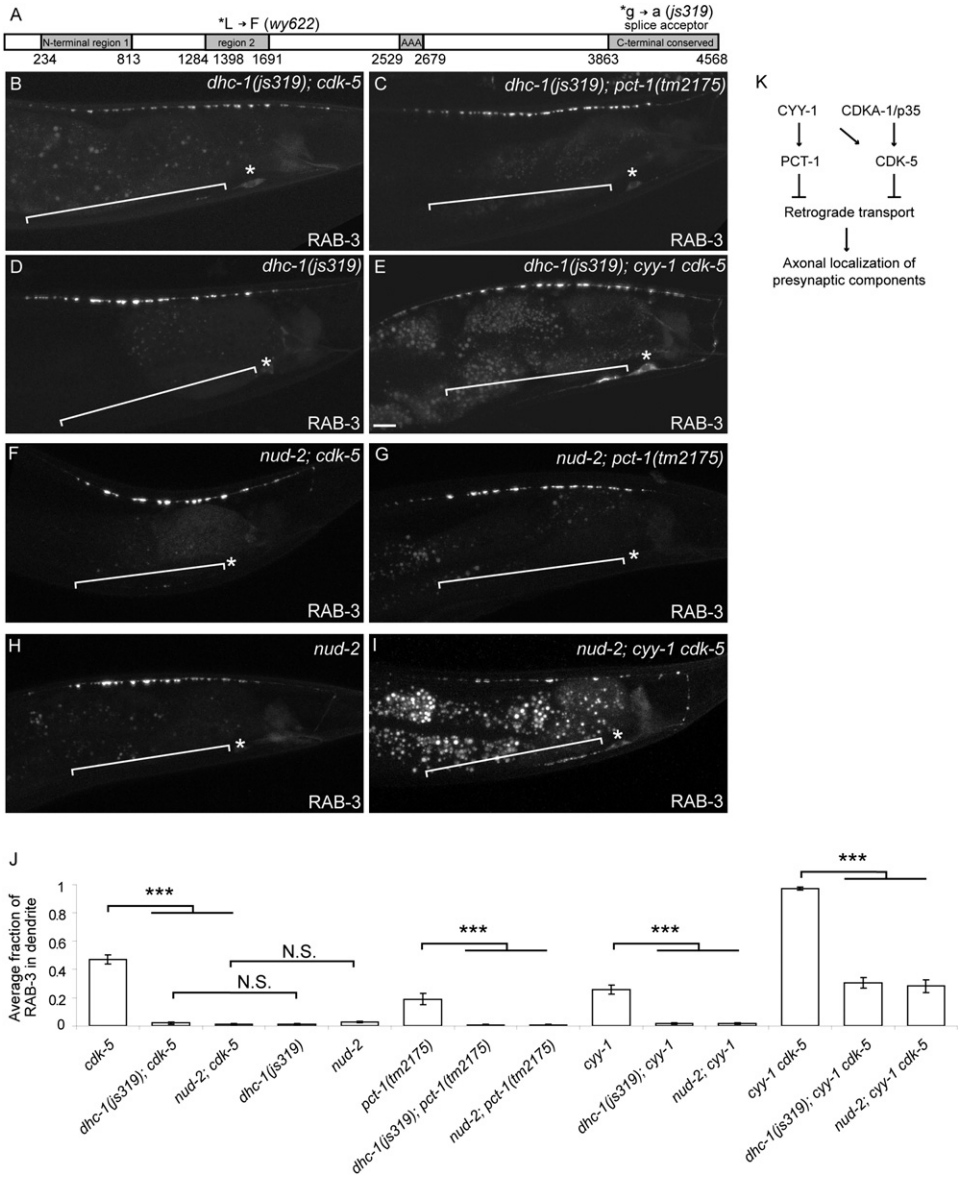

Figure 7. Loss-of-Function Mutations in Dynein Suppress the Mislocalization Defect in the CDK Mutants

(A) Schematic diagram of DHC-1 protein and mutations. The main domains are N-terminal region 1, N-terminal region 2, a domain conserved among the ATPase family associated with various cellular activities (AAA), and a C-terminal conserved region.

(B–I) Representative confocal micrographs of GFP::RAB-3 in DA9 (*wyIs85)* of different genotypes. *dhc-1(js319); cdk-5* (B), *dhc-1(js319); pct-1* (C), *dhc-1(js319)* (D), *dhc-1(js319); cyy-1 cdk-5* (E), *nud-2; cdk-5* (F), *nud-2; pct-1* (G), *nud-2* (H) and *nud-2; cyy-1 cdk-5* (I). (J) Graph of severity of GFP::RAB-3 mislocalization. Error bars represent SEM n = 20. ***p < 0.0005. t test. (K) Model of the two CDK pathways.

to be determined if mammalian cyclin Y activates Pctaire kinases.

Another upstream activator of Pctaire1 that has been characterized is CDK-5 (Liu et al., 2006). However, the *C. elegans* PCT-1 protein lacks the phosphorylation site for CDK-5 and is unlikely to be its substrate. With regards to downstream substrates, Pctaire1 has been shown to phosphorylate N-Ethylmaleimide-sensitive fusion protein, a factor important for membrane fusion (Cheng et al., 2002; Liu et al., 2006). Pctaire1 also interacts with p11/calpactin I light chain and 14-3-3, both of which are associated with multiple factors including c-kinase, Raf, Bcr, and PI3-kinase, but none of them have been identified as a substrate of Pctaire kinases (Le Bouffant et al., 1998). Due to the limited information available about the substrates of Pctaire kinases, it is hard to deduce a consensus substrate motif. However, similar to other CDKs or CDK-5, they likely phosphorylate the sequence (S/T)PX(K/H/R) (Liu et al., 2006). Further understanding of other features common to substrates of Pctaire kinases is needed to elucidate the mechanism of its function.

CDKs and Axonal Transport

In contrast to Pctaire kinases and cyclin Y, the proline-directed serine threonine kinase CDK-5 has been studied extensively and has been implicated in many aspects of neuronal development, such as neuronal migration, neurite outgrowth, synaptic formation, and neuronal survival (Gilmore et al., 1998; Kwon and Tsai, 1998; Ohshima et al., 1996; Yip et al., 2007). Astonishingly large numbers of putative CDK-5 substrates have been identified and these substrates are associated with cytoskeletal structures including MTs, as well as membrane dynamics and synaptic assembly (Cheung et al., 2006; Samuels et al., 2007; Smith, 2003; Xie et al., 2006). Among these, what might mediate the effect of CDK-5 or its related kinase PCT-1 on axonal trafficking?

Proper localization of presynaptic components involves multiple steps, including MT-based transport over long distances and local assembly at presynaptic specializations. As CDK-5 phosphorylates multiple MT-associated proteins and Pctaire3 indirectly phosphorylates tau (Herskovits and Davies, 2006), the CDKs may regulate the localization of presynaptic components by reorganizing the cytoskeleton. We did not detect major alterations to MT polarity and general axon morphology when both CDK pathways are disrupted, suggesting that cytoskeletal rearrangement is unlikely to be the major or only cause of mislocalized presynaptic components. However, our assay for MT polarity might not be sensitive enough to detect subtle changes of polarity.

CDK-5 was recently shown to recruit the MAGUK family member CASK, an active zone protein that interacts with calcium channels and multiple adaptor proteins, to presynaptic sites (Samuels et al., 2007). In *C. elegans*, the phenotype of a strong assembly defect in DA9 is distinct from the defect in mutants in the two CDK pathways (Figure S5S-T). Therefore, while CDK-5 might also affect the local assembly of presynaptic specializations in DA9, it is unlikely that the CDKs maintain proper localization of presynaptic components solely through regulating synapse assembly.

Our genetic and cell biology experiments suggest that the CDK pathways affect intracellular trafficking by regulating motor proteins. Several studies support the involvement of CDK-5 or its related kinase in axonal transport. First, in the squid giant axon, the CDK inhibitor olomoucin affects fast anterograde movement while substrates for proline-directed kinases like KSPXK peptide and histone H1 decrease both anterograde and retrograde transport (Ratner et al., 1998). Second, adding the CDK inhibitor olomoucin or knocking out CDK-5 activators p35 or p39 increases kinesin light chain phosphorylation, which may cause cargo release and the slowing down of fast anterograde axonal transport of membrane-bound organelles (Morfini et al., 2004; Morfini et al., 2002). Third and most relevant to this study, a series of elegant biochemistry studies showed that CDK-5 phosphorylates Nudel, a factor that associates with the retrograde motor dynein and its regulator LIS1 and this phosphorylation event regulates neuronal migration and neurite morphology (Niethammer et al., 2000; Sasaki et al., 2000). Taken together, CDK-5 and its related kinases regulate the balance of anterograde and retrograde motors. Since the defect of SVP localization can be restored largely by the *dhc-1* and *nud-2* mutations (Figure 7), we propose that CDK-5 and PCT-1 mainly repress retrograde transport to localize presynaptic components to axons and this may occur through the dynein complex.

Interactions between PCT-1/CYY-1 and CDK-5/p35

Our genetic double mutant analysis showed that PCT-1 and CYY-1 function in the same genetic pathway, while CDK-5 and CDKA-1/p35 act together. This notion is supported by the fact that CYY-1 binds directly to PCT-1 and is required for the kinase activity of PCT-1 in vitro. However, CYY-1 might also stimulate the activity of the CDK-5 pathway as a CYY-1 transgene can rescue the *pct-1* mutant but not *pct-1 cdk-5* double mutants. CDK-5 and its activators p35 and p39 are evolutionarily conserved across eukaryotic species and no cyclin-like activators of CDK-5 have been characterized. It is intriguing that our genetic studies suggest that the CYY-1 can act upstream of CDK-5 and its activator CDKA-1/p35. Moreover, although canonical cyclins cannot affect CDK-5 activity, they can still bind CDK-5 (Miyajima et al., 1995; Yip et al., 2007). Consistent with our genetic analysis, we found that CYY-1 can efficiently stimulate CDK-5 kinase activity in vitro. How CYY-1 regulates PCT-1 and CDK-5 to target presynaptic components in a spatially specific manner is worth investigating, especially since other cyclins generally behave as temporal regulators.

EXPERIMENTAL PROCEDURES

Strains and Genetics

Worms were raised on OP50 *E. coli* seeded NGM plates at 22°C. The following mutant strains were obtained through the Caenorhabditis Genetics Center: RB814 *cdk-5(ok626)III*, CB1265 *unc-104(e1265)II*, RB1471 *pct-1(ok1707)IV,* WM99 *cdk-1(ne2257)II,* JH1288 *cdk-7(ax224I)*, CZ1893 *syd-1(ju82)II*, and RB1022 *nud-2(ok949)I*. FX00648 *cdka-1(tm648)III*, FX02175 *pct-1(tm2175)IV*, and FX01238 *cdk-8(tm1238)I* were kindly provided by Shohei Mitani. NM1489 *dhc-1(js319); jsIs37* was kindly provided by Mike Nonet. TV74 *syd-2(wy5)X,* a null allele(Chao, unpublished), and TV6851 *unc-104(e1265wy565),* a weak allele (K.S., unpublished data) was previously isolated from our lab. N2 Bristol was utilized as the wild-type reference strain.

Genetic Screens

wy575 was isolated from an F2 semiclonal visual screen of 600 haploid genomes for *lin-44/wnt(n1792); wyIs85* enhancers. *wy302* was isolated from an F2 semiclonal visual screen of 3000 haploid genomes from the *wyIs109* strain. *wy622* was isolated from an F2 semiclonal visual screen of 3000 haploid genomes for *cdk-5(ok626); wyIs85* enhancers. *wy565* was isolated from an F2 behavioral screen of 1200 haploid genomes for *unc-104(e1265); wyIs87* suppressors. Worms were mutagenized with 50 mM EMS.

Cloning and Constructs

Expression clones were made in a derivative of pPD49.26 (A. Fire, personal communication), the pSM vector (S. McCarroll and C. I. Bargmann, personal communication). The plasmids and strains were generated as previously described (Klassen and Shen, 2007; Margeta et al., 2009). We utilized the co-injection markers P*odr-1::GFP* or *dsRED* injected at 20ng μl^{-1} and transgenes were introduced into *C. elegans* as previously described (Mello and Fire, 1995).

Fluorescence Microscopy and Confocal Imaging

Images of fluorescently-tagged fusion proteins were captured in live *C. elegans* using a Plan-Apochromat 63X/1.4 objective on a Zeiss LSM510 or LSM710 confocal microscope. Worms were immobilized using 1.25mM levamisole (Sigma) and 112.5mM 2,3-butanedione monoxime (Sigma).

Electron Microscopy

N2 and *cyy-1 cdk-5* animals were processed for electron microscopy essentially as previously described (Hammarlund et al., 2007) and supplement methods. A total of ~12μm segments were reconstructed for each strain and annotated using ImageJ. The DA, DB, and DD neurons were recognized by their orientation pattern (White et al., 1986). A varicosity was defined as a series of profiles with an area larger than 10,000 square nm. In N2 animals, seven DA, six DB, and five DD varicosities were analyzed. In *cyy-1 cdk-5* double mutants, eight DA, four DB, and six DD varicosities were analyzed.

Dynamic Imaging

Dynamic imaging was performed on the inverted Zeiss Axio Observer Z1 microscope equipped with the highly sensitive QuantEM:512SC camera. A Plan-Apochromat 63X/1.4 objective was used for acquisition.

L4 worms were cultured at 25°C for imaging. They were mounted onto 2% agarose pads and anesthetized with 6mM levamisol (Sigma) for no longer than 20min.

All movies were acquired over 40 s with 7 frames per second and an illumination time of 100ms. Movies were then analyzed using the ImageJ software.

Coimmunoprecipitation and Kinase Activity Assays

Mammalian expression constructs encoding *C. elegans* CYY-1-FLAG and PCT-1-HA were overexpressed in HEK293T cells by lipofectamine plus (Invitrogen) and coimmunoprecipated by anti-FLAG (Sigma) or anti-HA (Roche) antibodies (2 μg) as previously described (Fu et al., 2007).

For in vitro kinase assays, mammalian expression constructs encoding *C. elegans* CYY-1-FLAG with PCT-1-HA or CDK-5-HA were overexpressed in HEK293T cells as previously described (Cheng et al., 2002). The PCT-1 or CDK-5 complex was coimmunoprecipitated using anti-HA antibody (Santa Cruz). Recombinant myelin basic protein (0.5 mg; Calbiochem) or recombinant Histone H1 protein (5 μg; Calbiochem) was used as a substrate for PCT-1 or CDK-5 respectively in the in vitro kinase assays.

SUPPLEMENTAL INFORMATION

Supplemental Information includes Extended Experimental Procedures and six figures and can be found with this article online at doi:10.1016/j.cell.2010.04.011.

ACKNOWLEDGMENTS

This work was supported by the Human Frontier Science Foundation, the W.M. Keck Foundation, and the Howard Hughes Medical Institute. We thank the International *C. elegans* Gene Knockout Consortium, the National Bioresource Project-Japan, and the Nonet lab for strains. We also thank Y. Wu, M. Margeta, C. Gao, and Y. Fu for technical assistance, and C. Bargmann, L.H. Tsai, and members of the Shen lab for thoughtful comments on the manuscript.

Received: August 21, 2009
Revised: January 14, 2010
Accepted: April 6, 2010
Published: May 27, 2010

REFERENCES

Baas, P.W., Deitch, J.S., Black, M.M., and Banker, G.A. (1988). Polarity orientation of microtubules in hippocampal neurons: uniformity in the axon and nonuniformity in the dendrite. Proc. Natl. Acad. Sci. USA *85*, 8335–8339.

Burack, M.A., Silverman, M.A., and Banker, G. (2000). The role of selective transport in neuronal protein sorting. Neuron *26*, 465–472.

Cai, Q., Pan, P.Y., and Sheng, Z.H. (2007). Syntabulin-kinesin-1 family member 5B-mediated axonal transport contributes to activity-dependent presynaptic assembly. J. Neurosci. *27*, 7284–7296.

Cheng, K., Li, Z., Fu, W.Y., Wang, J.H., Fu, A.K., and Ip, N.Y. (2002). Pctaire1 interacts with p35 and is a novel substrate for Cdk5/p35. J. Biol. Chem. *277*, 31988–31993.

Cheung, Z.H., Fu, A.K., and Ip, N.Y. (2006). Synaptic roles of Cdk5: implications in higher cognitive functions and neurodegenerative diseases. Neuron *50*, 13–18.

Fejtova, A., Davydova, D., Bischof, F., Lazarevic, V., Altrock, W.D., Romorini, S., Schone, C., Zuschratter, W., Kreutz, M.R., Garner, C.C., et al. (2009). Dynein light chain regulates axonal trafficking and synaptic levels of Bassoon. J. Cell Biol. *185*, 341–355.

Fu, W.Y., Chen, Y., Sahin, M., Zhao, X.S., Shi, L., Bikoff, J.B., Lai, K.O., Yung, W.H., Fu, A.K., Greenberg, M.E., et al. (2007). Cdk5 regulates EphA4-mediated dendritic spine retraction through an ephexin1-dependent mechanism. Nat. Neurosci. *10*, 67–76.

Furukawa, Y., Kikuchi, J., Nakamura, M., Iwase, S., Yamada, H., and Matsuda, M. (2000). Lineage-specific regulation of cell cycle control gene expression during haematopoietic cell differentiation. Br. J. Haematol. *110*, 663–673.

Garrido, J.J., Fernandes, F., Giraud, P., Mouret, I., Pasqualini, E., Fache, M.P., Jullien, F., and Dargent, B. (2001). Identification of an axonal determinant in the C-terminus of the sodium channel Na(v)1.2. EMBO J. *20*, 5950–5961.

Gilmore, E.C., Ohshima, T., Goffinet, A.M., Kulkarni, A.B., and Herrup, K. (1998). Cyclin-dependent kinase 5-deficient mice demonstrate novel developmental arrest in cerebral cortex. J. Neurosci. *18*, 6370–6377.

Graeser, R., Gannon, J., Poon, R.Y., Dubois, T., Aitken, A., and Hunt, T. (2002). Regulation of the CDK-related protein kinase PCTAIRE-1 and its possible role in neurite outgrowth in Neuro-2A cells. J. Cell Sci. *115*, 3479–3490.

Hall, D.H., and Hedgecock, E.M. (1991). Kinesin-related gene unc-104 is required for axonal transport of synaptic vesicles in C. elegans. Cell *65*, 837–847.

Hammarlund, M., Palfreyman, M.T., Watanabe, S., Olsen, S., and Jorgensen, E.M. (2007). Open syntaxin docks synaptic vesicles. PLoS Biol. *5*, e198.

Herskovits, A.Z., and Davies, P. (2006). The regulation of tau phosphorylation by PCTAIRE 3: implications for the pathogenesis of Alzheimer's disease. Neurobiol. Dis. *23*, 398–408.

Hirokawa, N., and Takemura, R. (2005). Molecular motors and mechanisms of directional transport in neurons. Nat. Rev. Neurosci. *6*, 201–214.

Horton, A.C., and Ehlers, M.D. (2003). Neuronal polarity and trafficking. Neuron *40*, 277–295.

Kiess, M., Gill, R.M., and Hamel, P.A. (1995). Expression of the positive regulator of cell cycle progression, cyclin D3, is induced during differentiation of myoblasts into quiescent myotubes. Oncogene *10*, 159–166.

Klassen, M.P., and Shen, K. (2007). Wnt signaling positions neuromuscular connectivity by inhibiting synapse formation in C. elegans. Cell *130*, 704–716.

Koushika, S.P., Schaefer, A.M., Vincent, R., Willis, J.H., Bowerman, B., and Nonet, M.L. (2004). Mutations in Caenorhabditis elegans cytoplasmic dynein components reveal specificity of neuronal retrograde cargo. J. Neurosci. *24*, 3907–3916.

Kwon, Y.T., and Tsai, L.H. (1998). A novel disruption of cortical development in p35(−/−) mice distinct from reeler. J. Comp. Neurol. *395*, 510–522.

Le Bouffant, F., Capdevielle, J., Guillemot, J.C., and Sladeczek, F. (1998). Characterization of brain PCTAIRE-1 kinase immunoreactivity and its interactions with p11 and 14-3-3 proteins. European Journal of Biochemistry / FEBS *257*, 112–120.

Lew, J., Huang, Q.Q., Qi, Z., Winkfein, R.J., Aebersold, R., Hunt, T., and Wang, J.H. (1994). A brain-specific activator of cyclin-dependent kinase 5. Nature *371*, 423–426.

Liu, Y., Cheng, K., Gong, K., Fu, A.K., and Ip, N.Y. (2006). Pctaire1 phosphorylates N-ethylmaleimide-sensitive fusion protein: implications in the regulation of its hexamerization and exocytosis. J. Biol. Chem. *281*, 9852–9858.

Ma, S., and Chisholm, R.L. (2002). Cytoplasmic dynein-associated structures move bidirectionally in vivo. J. Cell Sci. *115*, 1453–1460.

Margeta, M.A., Wang, G.J., and Shen, K. (2009). Clathrin adaptor AP-1 complex excludes multiple postsynaptic receptors from axons in C. elegans. Proc. Natl. Acad. Sci. USA *106*, 1632–1637.

Mello, C., and Fire, A. (1995). DNA transformation. Methods Cell Biol. *48*, 451–482.

Meyyappan, M., Wong, H., Hull, C., and Riabowol, K.T. (1998). Increased expression of cyclin D2 during multiple states of growth arrest in primary and established cells. Mol. Cell. Biol. *18*, 3163–3172.

Miyajima, M., Nornes, H.O., and Neuman, T. (1995). Cyclin E is expressed in neurons and forms complexes with cdk5. Neuroreport *6*, 1130–1132.

Morfini, G., Szebenyi, G., Brown, H., Pant, H.C., Pigino, G., DeBoer, S., Beffert, U., and Brady, S.T. (2004). A novel CDK5-dependent pathway for regulating GSK3 activity and kinesin-driven motility in neurons. EMBO J. *23*, 2235–2245.

Morfini, G., Szebenyi, G., Elluru, R., Ratner, N., and Brady, S.T. (2002). Glycogen synthase kinase 3 phosphorylates kinesin light chains and negatively regulates kinesin-based motility. EMBO J. *21*, 281–293.

Niethammer, M., Smith, D.S., Ayala, R., Peng, J., Ko, J., Lee, M.S., Morabito, M., and Tsai, L.H. (2000). NUDEL is a novel Cdk5 substrate that associates with LIS1 and cytoplasmic dynein. Neuron *28*, 697–711.

Ohshima, T., Ward, J.M., Huh, C.G., Longenecker, G., Veeranna, Pant, H.C., Brady, R.O., Martin, L.J., and Kulkarni, A.B. (1996). Targeted disruption of the cyclin-dependent kinase 5 gene results in abnormal corticogenesis, neuronal pathology and perinatal death. Proc. Natl. Acad. Sci. USA *93*, 11173–11178.

Pack-Chung, E., Kurshan, P.T., Dickman, D.K., and Schwarz, T.L. (2007). A Drosophila kinesin required for synaptic bouton formation and synaptic vesicle transport. Nat. Neurosci. *10*, 980–989.

Poon, V.Y., Klassen, M.P., and Shen, K. (2008). UNC-6/netrin and its receptor UNC-5 locally exclude presynaptic components from dendrites. Nature *455*, 669–673.

Ratner, N., Bloom, G.S., and Brady, S.T. (1998). A role for cyclin-dependent kinase(s) in the modulation of fast anterograde axonal transport: effects defined by olomoucine and the APC tumor suppressor protein. J. Neurosci. *18*, 7717–7726.

Sampo, B., Kaech, S., Kunz, S., and Banker, G. (2003). Two distinct mechanisms target membrane proteins to the axonal surface. Neuron *37*, 611–624.

Samuels, B.A., Hsueh, Y.P., Shu, T., Liang, H., Tseng, H.C., Hong, C.J., Su, S.C., Volker, J., Neve, R.L., Yue, D.T., et al. (2007). Cdk5 promotes synaptogenesis by regulating the subcellular distribution of the MAGUK family member CASK. Neuron *56*, 823–837.

Sasaki, S., Shionoya, A., Ishida, M., Gambello, M.J., Yingling, J., Wynshaw-Boris, A., and Hirotsune, S. (2000). A LIS1/NUDEL/cytoplasmic dynein heavy chain complex in the developing and adult nervous system. Neuron *28*, 681–696.

Sato-Yoshitake, R., Yorifuji, H., Inagaki, M., and Hirokawa, N. (1992). The phosphorylation of kinesin regulates its binding to synaptic vesicles. J. Biol. Chem. *267*, 23930–23936.

Setou, M., Nakagawa, T., Seog, D.H., and Hirokawa, N. (2000). Kinesin superfamily motor protein KIF17 and mLin-10 in NMDA receptor-containing vesicle transport. Science *288*, 1796–1802.

Sieburth, D., Ch'ng, Q., Dybbs, M., Tavazoie, M., Kennedy, S., Wang, D., Dupuy, D., Rual, J.F., Hill, D.E., Vidal, M., et al. (2005). Systematic analysis of genes required for synapse structure and function. Nature *436*, 510–517.

Smith, D. (2003). Cdk5 in neuroskeletal dynamics. Neurosignals *12*, 239–251.

Tomizawa, K., Ohta, J., Matsushita, M., Moriwaki, A., Li, S.T., Takei, K., and Matsui, H. (2002). Cdk5/p35 regulates neurotransmitter release through phosphorylation and downregulation of P/Q-type voltage-dependent calcium channel activity. J. Neurosci. *22*, 2590–2597.

Tsai, L.H., Delalle, I., Caviness, V.S., Jr., Chae, T., and Harlow, E. (1994). p35 is a neural-specific regulatory subunit of cyclin-dependent kinase 5. Nature *371*, 419–423.

Uchida, T., Ishiguro, K., Ohnuma, J., Takamatsu, M., Yonekura, S., and Imahori, K. (1994). Precursor of cdk5 activator, the 23 kDa subunit of tau protein kinase II: its sequence and developmental change in brain. FEBS Lett. *355*, 35–40.

Vale, R.D. (2003). The molecular motor toolbox for intracellular transport. Cell *112*, 467–480.

White, J.G., Southgate, E., Thomson, J.N., and Brenner, S. (1976). The structure of the ventral nerve cord of Caenorhabditis elegans. Philos. Trans. R. Soc. Lond. B Biol. Sci. *275*, 327–348.

White, J.G., Southgate, E., Thomson, J.N., and Brenner, S. (1986). The structure of the nervous system of the nematode caenorhabditis elegans. Philos. Trans. R. Soc. Lond. B Biol. Sci. *314*, 340.

Wisco, D., Anderson, E.D., Chang, M.C., Norden, C., Boiko, T., Folsch, H., and Winckler, B. (2003). Uncovering multiple axonal targeting pathways in hippocampal neurons. J. Cell Biol. *162*, 1317–1328.

Xie, Z., Samuels, B.A., and Tsai, L.H. (2006). Cyclin-dependent kinase 5 permits efficient cytoskeletal remodeling–a hypothesis on neuronal migration. Cereb. Cortex *16* (*Suppl 1*), i64–i68.

Yamochi, T., Nishimoto, I., Okuda, T., and Matsuoka, M. (2001). ik3-1/Cables is associated with Trap and Pctaire2. Biochem. Biophys. Res. Commun. *286*, 1045–1050.

Yap, C.C., Wisco, D., Kujala, P., Lasiecka, Z.M., Cannon, J.T., Chang, M.C., Hirling, H., Klumperman, J., and Winckler, B. (2008). The somatodendritic endosomal regulator NEEP21 facilitates axonal targeting of L1/NgCAM. J. Cell Biol. *180*, 827–842.

Yip, Y.P., Capriotti, C., Drill, E., Tsai, L.H., and Yip, J.W. (2007). Cdk5 selectively affects the migration of different populations of neurons in the developing spinal cord. J. Comp. Neurol. *503*, 297–307.

Zahn, T.R., Angleson, J.K., MacMorris, M.A., Domke, E., Hutton, J.F., Schwartz, C., and Hutton, J.C. (2004). Dense core vesicle dynamics in Caenorhabditis elegans neurons and the role of kinesin UNC-104. Traffic *5*, 544–559.

EXTENDED EXPERIMENTAL PROCEDURES

Constructs and Transgenic Worms.

wyEx2288,9, 2776,7: a AscI-KpnI PCR fragment containing the *cyy-1* genomic sequence was subcloned into P*mig-13::yfp::unc-5 3′utr* pSM to make P*mig-13::cyy-1 stop::yfp::unc-5 3′utr*. A SphI-AscI PCR fragment containing P*itr-1 pB* was subcloned into *cyy-1stop::yfp::unc-5 3′utr* pSM. P*itr-1 pB::cyy-1stop::yfp::unc-5 3′utr* was injected at 10ng μl-1(*wyEx2288,9*) or 20ng μl-1(*wyEx2276,7)* with P*odr-1::gfp* at 20ng μl^{-1} into *cyy-1;wyIs85* or *pct-1;wyIs85* animals. The four arrays are separate lines obtained from two injections.

P*itr-1 pB* primers 5′ GAAAGGGGCCGCCATCTATTCCAGAGTTCGTTCCCGAGC and 3′ CTTTCCGGCGCGCCCAATTCGTGT GCTTCCACCACCAC

cyy-1 primers 5′ GAAAGGGGCGCGCCATGGGAAATTCATCGTGTTGTCTG and 3′ GAAAGGGGTACCCTACGAGAGAACAGCCG-GATG

wyEx2506,7: an AscI-KpnI PCR fragment containing the *pct-1c* genomic sequence was subcloned into Pmig-13 delta pSM vector to make P*mig-13::pct-1c::unc-54 3′utr*. This construct was injected with P*odr-1::gfp* (both at 20ng μl^{-1}) into *wyIs85* animals. The two arrays are separate lines obtained from one injection. *pct-1c* primers 5′ GAAAGGGGCGCGCCGTATACTTTCTCATTTCCATCG and 3′ GAAAGGGGTACCGCATATTATCATTTTTCTGGG

wyEx2706: an AscI-KpnI PCR fragment containing the *pct-1a* cDNA obtained from the ORFeome project (http://worfdb.dfci.harvard.edu/) was subcloned into P*itr-1 pB::yfp::unc-5 3′utr* pSM to make P*itr-1 pB::pct-1a stop::yfp::unc-5 3′utr*. This construct was injected at 40ng μl^{-1} with P*odr-1::gfp* at 20ng μl^{-1} into *wyIs85* animals. *pct-1a* primers 5′ GAAAGGGGCGCGCCATGAAGAAGCT-TAAACG and 3′ GAAAGGGGTACCTAAGTGTGATGACTCGAAT

wyEx2904, 2923: An AscI PCR fragment obtained from pAC13, a generous gift from M. Chalfie, containing *mec-2 intron9* was subcloned into P*itr-1 pB::pct-1a::unc-5 3′utr(wyEx2904)* or P*mig-13::cdk-5::unc-54 3′utr(wyEx2923)*. Both plasmids were injected at 10ng μl^{-1} with P*odr-1::gfp* at 20 ng μl^{-1} into *pct-1; wyIs85* or *cdk-5; wyIs85* mutants. The two arrays are separate lines obtained from one injection. *mec-2 intron9* primers 5′ GAAAGGGGCGCGCCCACCGCCTAAAGTGTAAGTTTTC and 3′ GAAAGGGGCGCGCCGACGGTGGCTCCTCACTGAAAAC

wyEx2624,6: The *cdk-5* entry clone was obtained from the ORFeome project (http://worfdb.dfci.harvard.edu/) and cloned into the destination vector Pmig-13::gateway::yfp(Klassen and Shen, 2007) and P*mig-13::gfp::gateway* using the gateway strategy with LR clonase (Invitrogen) to make P*mig-13::cdk-5::yfp* and P*mig-13::gfp::cdk-5.* The AscI-Kpn-1 fragment containing *cdk-5* was subcl-oned into *mig-13::unc-54 3′utr* pSM and the resulting plasmid was injected at 5ng μl^{-1} with P*odr-1::gfp* at 20ng μl^{-1} into *cdk-5; wyIs85*. The two arrays are separate lines obtained from one injection.

wyEx2286,7: P*itr-1::cdk-5::unc-54 3′utr* was injected at 10ng μl^{-1} with P*odr-1::gfp* at 20ng μl^{-1} into *cdk-5; wyIs85* animals. The two arrays are separate lines obtained from one injection.

wyEx2860,1: a AscI-KpnI PCR fragment containing the *cdka-1* genomic sequence was subcloned into P*itr-1 pB::yfp::unc-5 3′utr* pSM and P*itr-1 pB::cdka-1 stop::yfp::unc-5 3′utr* was injected at 10ng μl^{-1} with P*odr-1::gfp* at 20ng μl^{-1} into *cdka-1; wyIs85* animals. The two arrays are separate lines obtained from one injection. *cdka-1* primers 5′ GAAAGGGGCGCGCCATGGGCGCAAATTT-GACGTC and 3′ GAAAGGGGTACCTCATTCGGAACTTGAACAATGCTTG

wyEx2774, 2160, 2789, 2460: P*mig-13::pct-1c::gfp* (cloned as *wyEx2506*, 20ng μl^{-1}) (*wyEx2774*), P*itr-1pB::cdk-5::yfp* (cloned as *wyEx2624*, 50ng μl^{-1}) (*wyEx2160*), P*itr-1pB::cyy-1::yfp* (cloned as *wyEx2288*, 50ng μl^{-1}) (coinject with P*itr-1pB::mCherry,* 20ng μl^{-1}), P*itr-1pB::cdka-1/p35::yfp* (cloned as *wyEx2860,* 15ng μl^{-1}) were injected with P*odr-1::gfp* at 20ng μl^{-1} into into wild-type animals.

wyEx2694,5: The *unc-104* entry clone was kindly provided by Dieter Klopfenstein and inserted into the destination vector P*mig-13::gateway* to make P*mig-13::unc-104.* The resulting plasmid was injected at 50ng μl^{-1} with P*odr-1::gfp* at 20ng μl^{-1} into *cyy-1 cdk-5; wyIs85* animals. The two arrays are separate lines obtained from one injection.

wyEx2992: a Nhe1-Kpn1 PCR fragment containing *unc-104(1-389)* sequence was subclone into *Pitr-1pB::GFP::unc-54 3′UTR pSM* to make P*itr-1 pB::unc-104(1-389)::gfp)*. This construct was injected at 20 ng μl^{-1} with P*odr-1::gfp* at 20ng μl^{-1} into into wild-type animals. *unc-104(1-389)* primers 5′ GAAAGGGCTAGCATGTCATCGGTTAAAGTAGCTG and 3′ GAAAGGGGTACCGTCTCCTG-TACGTCTGTGACA

wyEx3128: The *klp-16* entry clone was inserted into the destination vector P*itr-1 pB::gateway::yfp* to make P*itr-1 pB::klp-16::yfp.* The resulting plasmid was injected at 10ng μl^{-1} with P*odr-1::gfp* at 20ng μl^{-1} into wild-type animals.

wyEx2793: A SphI-AscI fragment containing P*mig-13* was subcloned into *gfp::rab-3::unc-54 3′utr* pSM and the resulting P*mig-13::gfp::rab-3* construct was injected at 4ng μl^{-1} with P*odr-1::gfp* at 40ng μl^{-1} into wild-type animals.

Electron Microscopy

Ten animals were placed in a type-A 100μm-deep specimen carrier (BAL-TEC) filled with bacteria and then capped with the flat side of a type-B specimen carrier. The specimens were frozen instantaneously in a BAL-TEC HPM 010 high-pressure freezer (BAL-TEC, Liechtenstein) and transferred into a cryovial containing anhydrous acetone with 1% osmium tetroxide, 0.1% uranyl acetate, and 1% water. Freeze-substitutions were carried out in a Leica EM AFS2 with the following program: 48 hr at −90°C, 5°C/hour to −20°C (14 hr), 16 hr at −20°C, and 10°C/hour to 20°C (4 hr). The animals were then infiltrated and embedded in epon-araldite. 200-300

contiguous ultra-thin (33 nm) sections were collected from regions around the anterior reflex of the gonad of multiple animals using an Leica Ultra 6 microtome. The sections were then stained with 2.5% uranyl acetate for 4 min and imaged on a Hitachi H-7100 electron microscope equipped with a GATAN orius CCD camera.

Temperature Shift Experiments

pct-1(tm2175);wyIs85; wyEx2904(Pitr-1pB::intron::pct-1) and *pct-1(tm2175);wyIs85* (Figure S6B) or *cdk-5(ok626); wyIs85; wyEx2904(Pitr-1pB::intron::cdk-5)*and *cdk-5(ok626); wyIs85* (Figure S6C) animals were cultured at 16°C or 25°C for multiple generations before being shifted to a different temperature. These animals in the L3 and early L4 larval stages were placed at 16°C for three days or at 25°C for two days before the phenotype was analyzed. Scoring was done in gravid adults.

Coimmunoprecipitation Assay

The cells were lysed in lysis buffer (in mM) (HEPES, [pH 7.4], 25; $MgCl_2$, 1; NaCl, 300; EDTA, 1; EGTA, 1) supplemented with 0.5% Nonidet P-40 and various protease inhibitors. The cell lysates were then incubated with anti-FLAG (Sigma) or anti-HA (Roche) antibodies (2 μg) at 4°C for 2 hr, followed by incubation with 40 μl of protein G sepharose (GE Healthcare) at 4°C for 1 hr. The samples were washed with lysis buffer and resuspended in SDS sample buffer. Proteins were coimmunoprecipitated and detected using western blot analysis.

In Vitro Kinase Assay

The cells were lysed using lysis buffer (HEPES, [pH 7.4], 25 mM; EGTA, 1 mM; DTT, 1 mM) supplemented with 0.2% Nonidet P-40 and various protease inhibitors.

The kinase assay was performed at 30°C for 30 min in kinase buffer (20 mM MOPS, [pH 7.4], 15 mM $MgCl_2$, 100 μM ATP) containing 1 μCi of [γ-^{32}P] ATP (PerkinElmer). Phosphorylated proteins were separated by 15% SDS-PAGE and visualized by autoradiography.

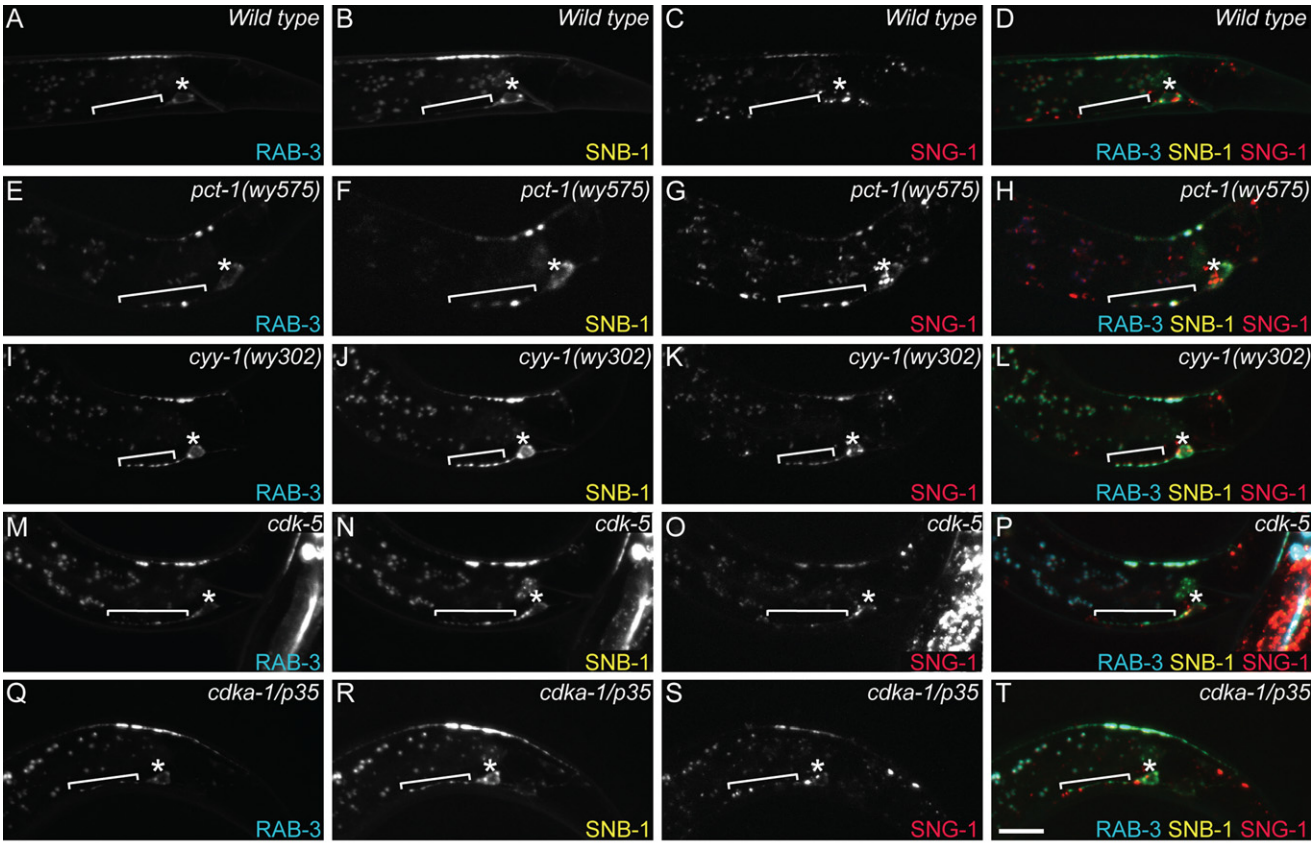

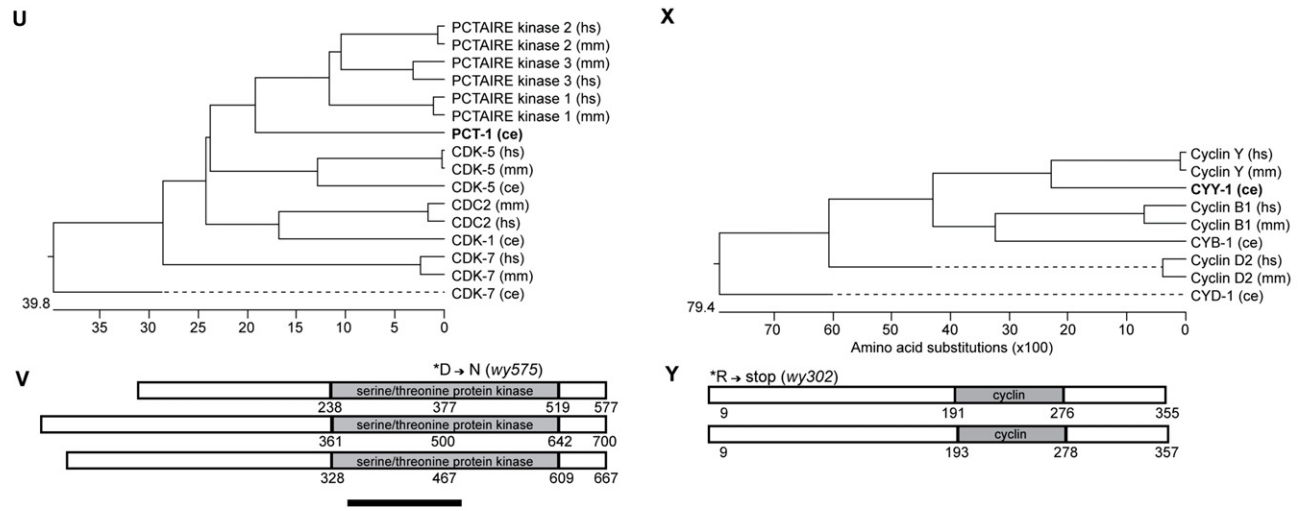

Figure S1. Mislocalization of Various Synaptic Vesicle Proteins in *wy575* and *wy302* Mutants and their Cloning, Related to Figure 1

(A–T) Synaptic vesicle proteins synaptobrevin/SNB-1, synaptogyrin/SNG-1 and RAB-3 mislocalize to the DA9 Dendrite in *pct-1(wy575), cyy-1(wy302), cdk-5(ok626),* and *cdka-1/p35(tm648)* Mutants. (A-D) Wild-type young larval L1 animal coexpressing CFP::RAB-3, SNB-1::YFP, and SNG-1::mCherry in DA9(-*wyIs109*). Note that all three markers are absent from the DA9 dendrite. (E-T) CFP::RAB-3, SNB-1::YFP, and SNG-1::mCherry in *pct-1(wy575)*, *cyy-1(wy302), cdk-5,* and *cdka-1/p35* mutant animals. The fluorescence in the middle of the worm is gut autofluorescence. Anterior, left and dorsal, top. Bracket, dendrite; asterisk, above cell body. The scale bar represents 10 μm.

(U–Y) Cloning of *wy575* and *wy302* mutants. (U) A balanced phylogenetic tree for PCT-1. (V) Schematic diagram of PCT-1 isoforms, *wy575* mutation, and *tm2175* deletion. (X) A balanced phylogenetic tree for CYY-1. CYB-1 and CYD-1 are *C. elegans* homologs of cyclin B and cyclin D respectively. (Y) Schematic diagram of CYY-1 isoforms and *wy302* mutation. Trees were generated using clustal analysis of full-length proteins in the software Megalign. The most closely related proteins from mouse (mm) and human (hs), and two known *C. elegans* cyclins and CDKs are included. Numbers in B and D indicate number of amino acids.

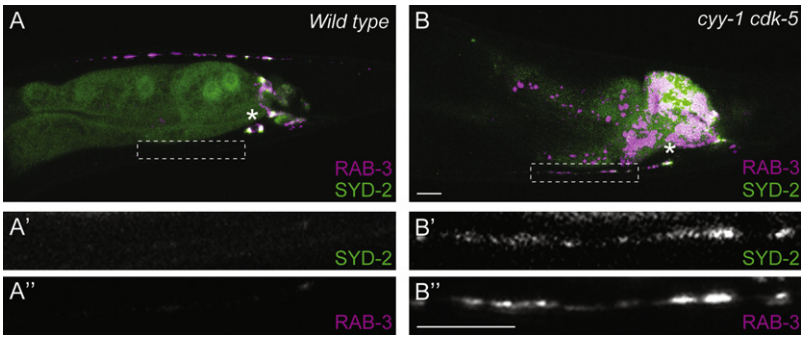

Figure S2. RAB-3 and SYD-2/Liprin-α Mislocalize to the DA9 Dendrite in *cyy-1 cdk-5* Mutant Animals, Related to Figure 2

(A and B) A wild-type (A) or *cyy-1 cdk-5* mutant animal (B) coexpressing GFP::RAB-3 and mCherry::SYD-2/liprin-α(*wyEx2055)* in DA9. (A'-B', A''-B'') Higher magnification micrographs of the corresponding dotted boxes. Asterisk, above cell body. The scale bar represents 10 μm.

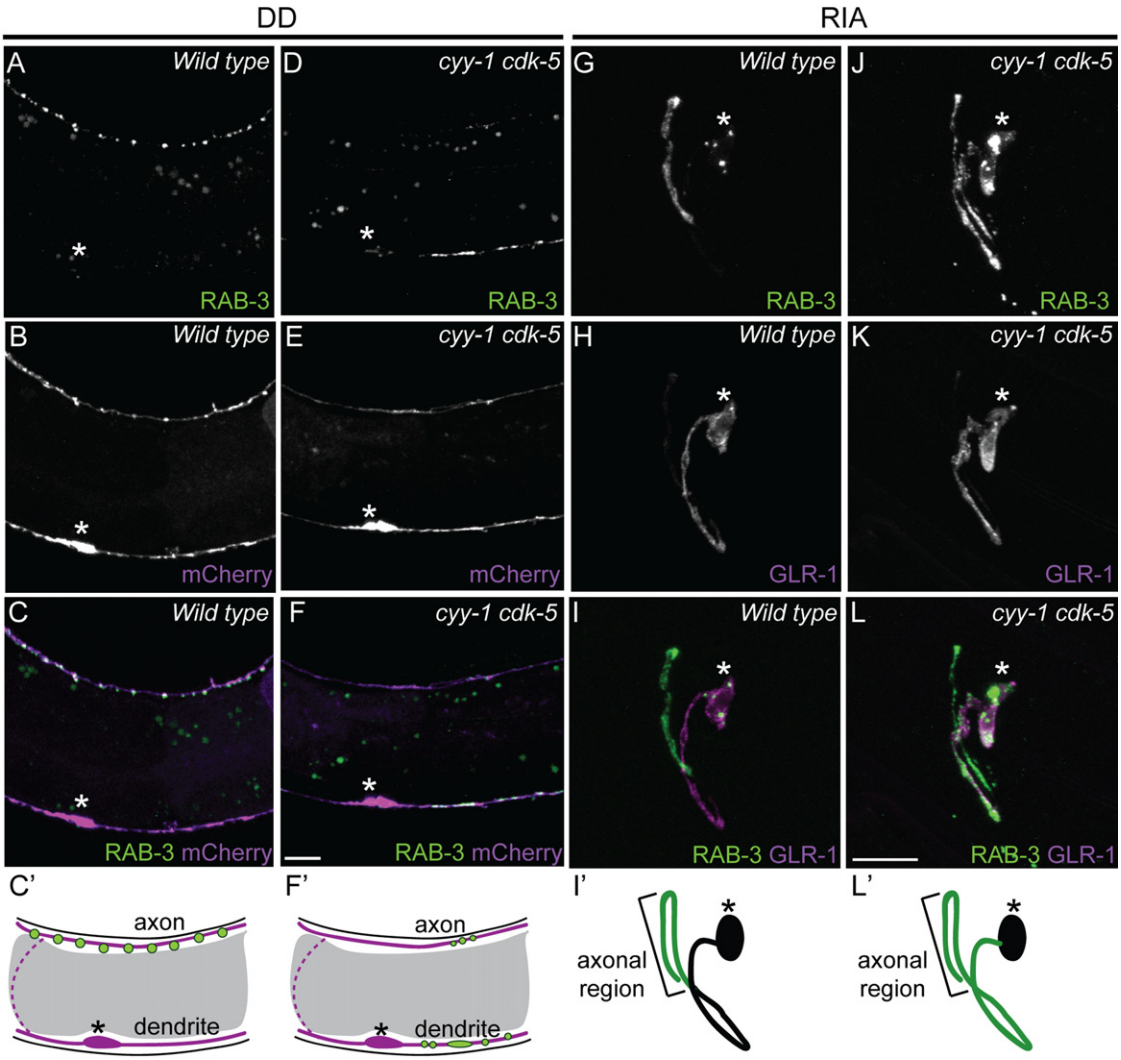

Figure S3. Synaptic Vesicle-Associated RAB-3 Mislocalizes to the Dendrite in DD and RIA Neurons in *cyy-1 cdk-5* Mutant Animals, Related to Figure 3

(A–F) Micrographs (A–C) and schematic diagram (C') of a wild-type adult animal coexpressing GFP::RAB-3 and mCherry in DD neurons(*wyIs202*). (D–F') GFP::RAB-3 and mCherry in a *cyy-1 cdk-5* mutant animal. (G–L') Micrographs and schematic diagram of wild-type (G–I') or *cyy-1 cdk-5* mutant animals (J-L') coexpressing mcherry::RAB-3 (green) and postsynaptic receptor GLR-1::GFP (purple) in RIA(*wyIs93*). GLR-1 is unaffected while RAB-3 is present in the post-synaptic domain of RIA. Asterisk above cell body. The scale bar represents 10 μm.

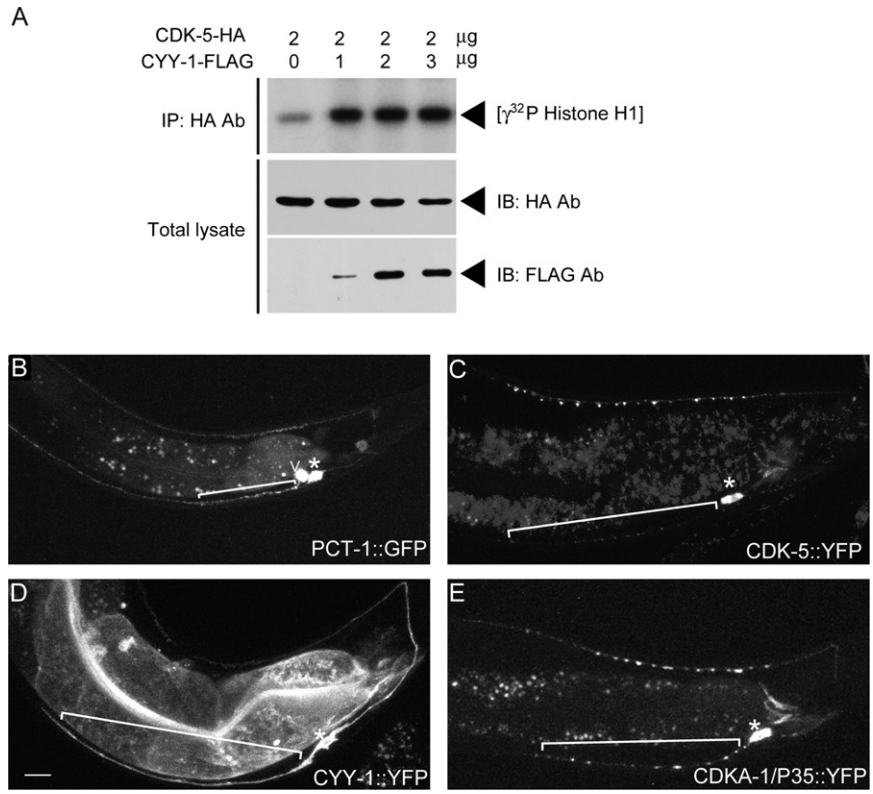

Figure S4. CYY-1 Can Activate CDK-5 and Subcellular Localization of PCT-1, CYY-1, CDK-5, and CDKA-1/p35, Related to Figure 4

(A) *C. elegans* CDK-5-HA and CYY-1-FLAG were coexpressed in HEK293T cells as indicated. Expression of CDK-5 alone exhibits no kinase activity, while coexpression with CYY-1 significantly increases the kinase activity of CDK-5. Lysate was immunoprecipitated with HA antibody and then subjected to kinase assay using Histone H1 protein as a substrate.

(B) PCT-1::GFP expressed in DA9 and VA12 neurons (*wyEx2774*).

(C) CDK-5::YFP expressed in DA9 (*wyEx2160*).

(D) CYY-1::YFP expressed in DA9 (*wyEx2789*).

(E) CDKA-1/p35::YFP expressed in DA9 (wyEx2460).

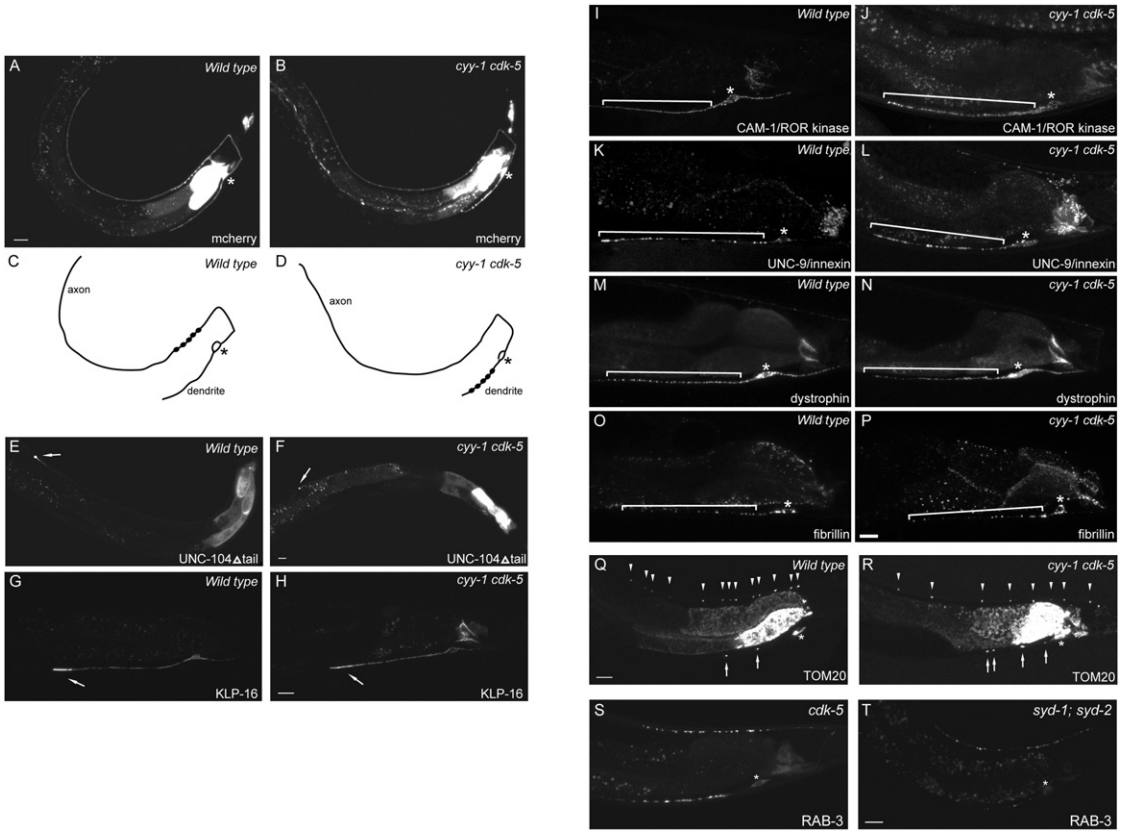

Figure S5. Many Aspects of Subcellular Specifications are Normal in *cyy-1 cdk-5* Mutants, Related to Figure 5

(A–D) DA9 axon and dendrite projection is normal in *cyy-1 cdk-5* mutant animals. Wild-type (A) or *cyy-1 cdk-5* (B) mutant animals expressing mCherry(*wyEx1902)* in DA9. (C, D) Schematic diagrams of DA9 guidance and morphology.(E-H) The anterograde motor UNC-104/KIF1A localizes to the tip of the dorsal axon while the minus-end Motor KLP-16/KIFC3 is enriched at the tip of the DA9 dendrite in wild-type and *cyy-1 cdk-5* Mutant Animals. This pattern is consistent with a mixed MT polarity in dendrite, where the preferred orientation is with their minus-ends oriented toward the tip of the dendrite. (E, F) Wild-type or *cyy-1 cdk-5* mutant animals expressing UNC-104 Δtail (1-389)::GFP(*wyEx2992)* in DA9. (G, H) Wild-type or *cyy-1 cdk-5* mutant animals expressing KLP-16::YFP(*wyEx3128)* in DA9. Arrow, accumulation of motor protein. (I-P) Four dendritic proteins localize appropriately in *cyy-1 cdk-5* Mutant Animals. Animals expressing CAM-1::YFP (I, J, *wyEx403*), UNC-9::YFP (K, L, *wyEx1054*), DYS-1::YFP (M, N, *wyEx2430*), or fibrillin::YFP (O, P, *wyEx2396*) in DA9. (Q-R) TOM20, a Subunit of the Mitochondrial Translocase Complex is Still Present in the Axon in *cyy-1 cdk-5* Mutant Animals. A wild-type (Q) or *cyy-1 cdk-5* mutant animal (R) expressing TOM20::YFP(*wyEx2406)* in DA9. Arrowheads, axonal TOM20 puncta. Arrows, dendritic TOM20 puncta. (S-T) Presynaptic assembly mutants have a different phenotype when compared to *cdk-5* Mutant Animals. A *cdk-5* (S) or *syd-1(ju82); syd-2/liprin-α(wy5)* mutant animal (T) expressing GFP:RAB-3(*wyIs85)* in DA9. Asterisk, indicates cell body. The scale bars represent 10 μm.

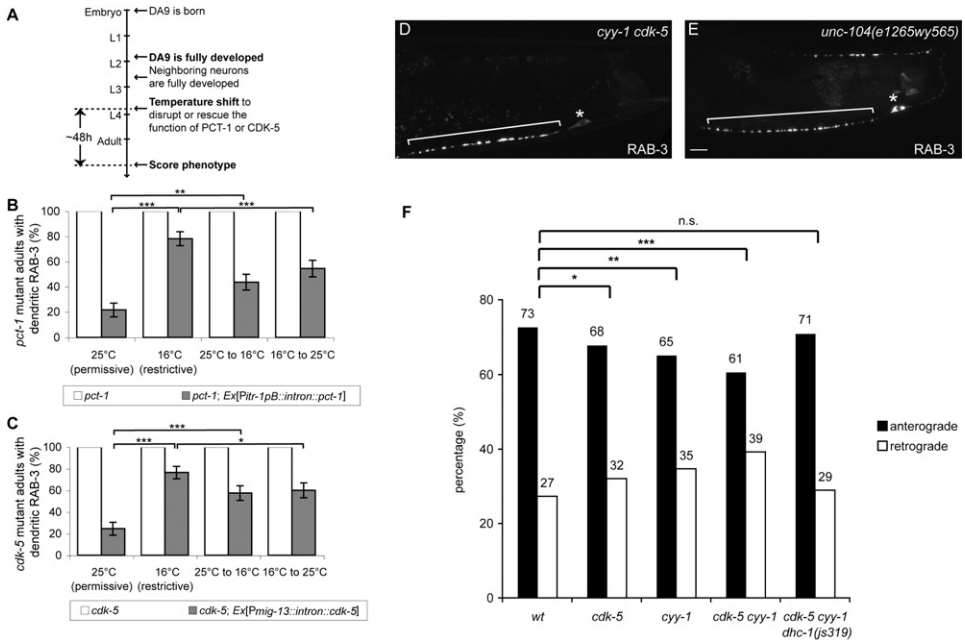

Figure S6. PCT-1 and CDK-5 Maintain the Balance between Anterograde and Retrograde SVP Transport, Related to Figure 6

(A–C) PCT-1 and CDK-5 are required to maintain the polarized localization of GFP::RAB-3. (A) Experimental time line. (B and C) *pct-1* (white columns in B) or *cdk-5* (white columns in C) mutant animals have mislocalized RAB3 in dendrites at 16-25°C. The mislocalization defect of *pct-1* or *cdk-5* mutant animals respectively is rescued at 25°C, not 16°C in early or later stage by $P_{itr\text{-}1pB}$*::intron::pct-1* (black columns in B, *wyEx2904*) or $P_{mig\text{-}13}$*::intron::cdk-5* (black columns in C, *wyEx2923*) transgenes. Error bars represent standard error of proportion. n > 100. ***p < 0.0005. **p < 0.005. *p < 0.05. χ^2 test.

(D and E) *unc-104/kif1a(e1265wy565)* mutants have a weaker mislocalization defect than *cyy-1 cdk-5* double mutants. A *cyy-1 cdk-5* double mutant animal (D) or *unc-104/kif1a(e1265wy565)* mutant animal (E) expressing GFP::RAB-3(*wyIs85*). Asterisk, below cell body. The scale bar represents 10 μm.

(F) Percentage of total SVPs moving in the anterograde (black) or retrograde (white) direction. While the balance between anterograde and retrograde transport is most dramatically affected in the *cdk-5 cyy-1* double mutant, either single mutant displays an intermediate phenotype significantly different from *wild-type* (*wt*). The *dhc-1(js319)* allele rescues the imbalance in SVP transport in the *cdk-5 cyy-1* mutant background. ***p < 0.0005; **p < 0.005; *p < 0.05, Fisher's exact test.